Functional Role for Cas Cytoplasmic Adaptor Proteins During Cortical Axon Pathfinding

Running title: Dual Functions of Cas Proteins in Cortical Tract Development

Jason A. Estep [1, *], Alyssa M. Treptow [1, *], Payton A. Rao [2], Patrick Williamson [3], Wenny Wong [2], Martin M. Riccomagno [1, 2, 3, #]

1 Cell, Molecular and Developmental Biology Graduate Program, Department of Molecular, Cell & Systems Biology, University of California, Riverside, CA, USA

2 Neuroscience Graduate Program, Department of Molecular, Cell & Systems Biology, University of California, Riverside, CA, USA

3 Neuroscience Undergraduate Program, Department of Molecular, Cell & Systems Biology, University of California, Riverside, CA, USA

* These authors contributed equally to this work

Corresponding Author: Martin M. Riccomagno, martinmr@ucr.edu.

Abstract

Proper neural circuit organization requires individual neurons to project to their targets with high specificity. While several guidance molecules have been shown to mediate axonal fasciculation and pathfinding, less is understood about how neurons intracellularly interpret and integrate these cues. Here we provide genetic evidence that the Crk-Associated Substrate (Cas) family of intracellular adaptor proteins is required for proper fasciculation and guidance of two cortical white matter tracts: the Anterior Commissure (AC) and thalamocortical axons (TCAs). Using a *Cas* Triple Conditional Knock Out (*Cas TcKO*) mouse model, we show that Cas proteins are required for proper TCA projection by a non-neuronal cortical cell population. We also demonstrate a requirement of the β1-integrin receptor for TCA projection, similarly in a population of non-neuronal cortical cells. Additional analysis of *Cas TcKO* mutants reveals a role for Cas proteins in AC fasciculation, here within the neurons themselves. This AC fasciculation requirement is not phenocopied in β1-integrin deficient mutants, suggesting that Cas proteins might signal downstream of a different receptor during this axon pathfinding event. These findings implicate Cas proteins as key mediators of cortical axon tract fasciculation and guidance.

Author Summary

In the developing nervous system, neurons extend axons—long projections that relay information to their targets—to establish neural circuits. Axons follow specific pathways directed by extracellular guidance cues, much like street signs direct traffic. While these guidance cues are well studied, how neurons internally interpret and respond to these signals

remains unclear. Here, we examine the role of the Crk-Associated Substrate (Cas) family of intracellular adaptor proteins in axon guidance within cortical axon tracts. Using genetic techniques to selectively remove *Cas* gene function from specific cell types, we demonstrate that Cas proteins are required for proper fasciculation (bundling) of anterior commissure axons, acting directly within the projecting axons themselves. Additionally, Cas proteins are required for proper guidance of thalamocortical projections—axons connecting the thalamus with the cortex. However, in this case, Cas proteins do not act within projecting axons but instead direct target neurons to their final positions. We further show that the β1-integrin receptor is similarly required for thalamocortical axon projection. These findings provide genetic evidence for a critical role of Cas adaptor proteins in both fasciculation and guidance of cortical axon tracts.

Introduction

During Central Nervous System (CNS) development, axons often traverse complex routes to meet their synaptic targets, interacting with a diverse array of attractive, repulsive, and permissive cues [1,2]. One developmental mechanism proposed to ensure proper guidance of large tracts is the concept of “pioneer” versus “follower” axons [3–7]. In this framework, initial pioneering axons carve out stereotyped trajectories due to the presence of intermediate targets, or guidepost cells [8]. These pioneer axons then serve as tracks that subsequent follower axons may use to reach a common target. Both the guidepost-to-guidepost advancement of pioneering axons, as well as the regulated fasciculation and defasciculation of follower axons, require neurons to properly sense and respond to adhesive signals [9,10] in the

61 forms of cell-cell and cell-extracellular matrix (ECM) interactions. In the vertebrate nervous
62 system, two well-established examples of guidepost-assisted axonal guidance are
63 thalamocortical axon (TCA) projections [11,12] and the commissural tracts of the forebrain, such
64 as the Anterior Commissure (AC) [13]. However, the exact cellular and molecular mechanisms
65 that permit the timely interpretation of adhesive signals during TCA guidance or AC formation
66 remain to be elucidated.

67 During normal development, TCA projections are guided by a diverse array of secreted
68 gradients, guidepost populations, and intermediate targets as they navigate their way from the
69 thalamus to the developing neocortex [14–16]. In mice, TCAs, originating from the thalamus at
70 embryonic day 12 (E12), first turn dorsolaterally at the diencephalic–telencephalic boundary
71 (DTB), then fasciculate to form the internal capsule on E13 and advance through the subpallium
72 until they reach the pallial-subpallial boundary (PSPB) at E14 [12,17]. At the pallial-subpallial
73 boundary (PSPB), TCAs encounter corticofugal axons and arrest for two to three days before
74 entering the cortical plate, temporarily targeting a cortical region known as the subplate [18–
75 20]. Entry of thalamic axons into the cortical layers and coordinated target selection is facilitated
76 by the subplate, a developmentally transient population of the earliest-born telencephalic
77 neurons that serves as an intermediate target for TCA pathfinding [18,19,21–23]. By E18, TCAs
78 innervate the cortical plate through the intermediate zone and defasciculate to reach their
79 individual targets [12,15], arriving at the neocortex before their target layer (layer IV) is fully
80 formed. Recent studies suggest that TCAs help promote the specification of layer IV neurons as
81 the cortex develops [24].

82 The formation of commissural tracts in the forebrain is also known to involve the
83 assistance of additional intermediate targets, often in the form of transient midline glial
84 populations [25–28], such as the glial "tunnel" that facilitates the formation of the Anterior
85 Commissure [29,30]. The AC is composed of two tracts that share a midline crossing point.
86 Beginning at E14-E15 in mice, axons of the anterior AC (aAC) originate from the Anterior
87 Olfactory Nucleus and form reciprocal connections to each olfactory bulb, while axons of the
88 posterior AC (pAC) originate from the ventrolateral cortex and join with the stria terminalis to
89 form reciprocal connections between the two hemispheres [31,32]. Recent developmental
90 studies have identified a population of pioneering axons that precede primary fascicle
91 formation and midline crossing during pAC establishment and suggest a role for ECM molecules
92 in the sorting of aAC and pAC axons [33].

93 The Crk-Associated Substrate (Cas) family of signal adaptor proteins is comprised of four
94 paralogues: p130Cas (Bcar1), Cas-L (HEF1, NEDD9), Sin (EFS), and Cass4 [34,35]. All four Cas
95 paralogues have high sequence conservation and structure similarity with an N-terminal SH3-
96 domain, a central substrate domain containing 15 repeats of the Tyr-X-X-Pro (YxxP) motif, and a
97 serine-rich domain [35]. Upon upstream receptor activation, Cas proteins are phosphorylated
98 on tyrosine residues within the substrate domain, thus permitting docking of SH2- and PTB-
99 containing partners such as Crk, CrkL, Nck, and SHIPTP2 [34,36–39]. Biochemical studies have
100 demonstrated that Cas proteins are phosphorylated downstream of Integrin [40–42],
101 Dystroglycan [43], CXCL12/CXCR4 [44], Neuropilin [45], and Netrin [46] signaling.
102 Phosphorylation of Cas induces the assembly of the Cas-Crk-DOCK180 scaffold complex which
103 subsequently recruits and activates Rac GTPases, leading to local actin polymerization

104 [34,47,48]. In this way, Cas proteins act as an essential link between external adhesion signals
105 and the actin cytoskeleton, permitting cells to reorganize their actin network in response to
106 ECM engagement.

107 While *p130Cas*[36], *CasL* [49], and *Sin* [50] are all expressed in the embryonic nervous
108 system, *Cass4* expression appears to be restricted primarily to the lung, spleen, and blood cells,
109 with minimal brain expression [51]. Within the context of neurodevelopment, Cas proteins have
110 been shown to regulate motor axon fasciculation and projection in Drosophila [41], with similar
111 roles in the fasciculation and pathfinding of Dorsal Root Ganglion (DRG) axons in the
112 mammalian Peripheral Nervous System (PNS) [52]. In the mammalian CNS, Cas proteins play
113 additional roles during neuronal migration and axonal guidance events: Cas adaptor proteins
114 coordinate commissural projections in the spinal cord [46], organize Retinal Ganglion Cell
115 positioning in the mouse retina [42], and have been recently shown to participate in cortical
116 lamination [43].

117 In this study, we sought to investigate the potential roles of Cas proteins during the
118 formation of forebrain white matter tracts. Accordingly, we focused our investigation on the
119 three Cas family members with established expression and functional roles in neural
120 development (p130Cas, CasL, and Sin). Using conditional reverse genetics, we have found that
121 Cas proteins are required for proper guidance of TCA projections and fasciculation of pAC axons.
122 We demonstrate that the TCA projection phenotype is cortical-autonomous but non-neuronal-
123 autonomous (i.e., *Cas* genes function in a population of cortical non-neuronal cells to regulate
124 proper lamination), with mis-projecting TCA processes closely associating with misplaced
125 subplate and deep layer neurons. Further, we demonstrate a cortical- and neuronal-

126 autonomous role for *Cas* genes (i.e., *Cas* genes function in cortical neurons) during AC
127 fasciculation and show that defasciculating AC axons originate, in part, from the dorsolateral
128 cortex. Interestingly, defects in AC fasciculation are not phenocopied by β1-integrin mutants,
129 suggesting that Cas proteins act, at least in part, independently of β1-integrin during AC
130 formation.

131 **Results**

132 To investigate the potential roles of *Cas* family genes during cortical white matter tract
133 formation, we began by assessing the expression of the *Cas* family paralogues during cortical
134 development. We recently established that transcripts for the paralogues *p130Cas*, *CasL/Nedd9*,
135 and *Sin/Efs* are all expressed in the developing neocortex, with overlapping expression in the
136 subventricular and ventricular zones [43]. The *p130Cas* transcript is dynamically enriched in the
137 cortical plate at E12.5 and the intermediate zone at E14.5, consistent with expression in
138 postmitotic neurons that are projecting axons [43].

139 We next performed immunohistochemistry in Swiss Webster embryos at E14.5, E16.5,
140 and E18.5 for p130Cas protein and the cortical white matter marker Neural Cell Adhesion
141 Molecule L1 (NCAM-L1) (**Fig 1**) [53–55] and the radial glia marker Nestin (**S1 Fig**) [56,57]. At
142 E14.5, p130Cas signal was detected in the intermediate zone, cortical plate, and marginal zone
143 (**Fig 1C-C'**). p130Cas signal co-expressed with the radial glial cell (RGC) marker Nestin in the
144 cortical plate and at the pial surface where radial glial endfeet adhere to the basement
145 membrane (**S1B Fig**). High-magnification images show co-expression of p130Cas with the axonal
146 marker NCAM-L1 in the presumptive Anterior Commissure (AC) (**Fig 1B-B'**). At E16.5, p130Cas

147 protein was broadly expressed throughout the developing neocortex, with the most robust
148 signal observed in the marginal zone, subventricular zone, and intermediate zone (**Fig 1F-F'**).
149 Additional high-magnification images demonstrate p130Cas signal strongly co-expressed with
150 NCAM-L1 in the External Capsule (EC) (**Fig 1E**, white arrow) and the now midline-crossing AC
151 (**Fig 1E**, white arrowheads). By E18.5, p130Cas expression was diffusely expressed throughout
152 the cortical plate, with stronger expression in the subventricular zone (**Fig 1I**) and cortical white
153 matter tracts, including the corpus callosum, internal capsule, EC, and AC (**Fig 1G**). Clear co-
154 expression of p130Cas with NCAM-L1 was observed in the EC (**Fig 1H**, white arrow) and AC (**Fig**
155 **1H**, white arrowheads).

156 To better visualize axons originating from neurons expressing *p130Cas*, we took
157 advantage of the *p130Cas-EGFP-BAC* transgenic line generated by the GENSAT BAC transgenic
158 project [58]. These mice carry a bacterial artificial chromosome (BAC) containing an enhanced
159 green fluorescent protein (EGFP) expression cassette which is driven by the *p130Cas* promoter
160 along with its regulatory sequences, thereby causing all cells with *p130Cas* promoter activity to
161 accumulate cytosolic EGFP in a pattern that recapitulates endogenous gene expression [43,52].

162 We collected *p130Cas-EGFP-BAC* embryos at E14.5 and E16.5 and neonates at postnatal
163 day 0 (P0) and performed immunohistochemistry for EGFP and NCAM-L1 to visualize cortical
164 white matter tracts (**Fig 2**). At E14.5, we found *p130Cas*-driven EGFP signal overlapped with
165 NCAM-L1 in multiple areas: the cortical plate, the lateral cortex, and a group of fasciculating
166 axons forming the presumptive AC (**Fig 2A-A''**, white arrowheads). By E16.5, robust *p130Cas*-
167 driven EGFP signal was observed broadly in the cortical plate and the marginal zone (**Fig 2B-B'**).
168 EGFP signal was also detected in white matter, with clear expression in internal capsule axons,

169 the EC (**Fig 2B**, white arrow), and the midline-crossing AC (**Fig 2B**, white arrowheads). In
170 neonates (P0), we observed strong *p130Cas*-driven EGFP in all major cortical tracts including the
171 corpus callosum, striatum, EC, and AC (**Fig 2C-C''**, white arrow denotes EC and white
172 arrowheads denote AC). Higher-magnification images of *p130Cas-EGFP-BAC* neonates at the
173 pallial-subpallial boundary (PSPB) revealed many diffuse NCAM-L1+ processes innervating the
174 subpallium that were not expressing *p130Cas*-driven EGFP, although many EGFP+ cell bodies
175 occupied this region (**Fig 2D-D''**, white dotted line indicates pallial-subpallial boundary (PSPB)).
176 In the cingulate cortex, high-magnification images of P0 *p130Cas*-EGFP-BAC animals showed
177 robust expression of EGFP in the cortical plate and the corpus callosum (**Fig 2E-E''**).

178 Having confirmed the developmental expression of *Cas* genes during the formation of
179 cortical white matter, we next sought to test the requirement of Cas proteins during cortical
180 tract formation. Thus, we generated *Cas* triple conditional knockouts (*Cas TcKO*) [42,43,52] to
181 assess the broad requirements for Cas proteins (p130Cas, CasL, and Sin) during cortical tract
182 development. In brief, *Cas TcKO* animals bear homozygous null alleles for the Cas homologues
183 *CasL* (*CasL*$^{-/-}$) and *Sin* (*Sin*$^{-/-}$) while also harboring one floxed allele and one deletion (delta) allele
184 for *p130Cas* (*p130Cas*$^{fl/\Delta}$). Constitutive deletion of *p130Cas* results in early embryonic lethality
185 due to defects in cardiovascular development [59]. Thus, crossing TcKO animals to cell-specific
186 Cre-driver lines permits Cre-mediated excision of *p130Cas* in neural tissue only, allowing
187 embryos to survive through development.

188 To determine the requirement of *Cas* genes during cortical white matter tract formation,
189 we chose to first induce a broad deletion of *Cas* gene function by crossing *Cas TcKO* animals
190 with *Nestin-Cre* mice. *Nestin-Cre* drives early (E9.5) recombination in neural stem cells and

191 intermediate progenitors [60]. As such, *Nestin-Cre* is often employed to produce CNS-wide
192 deletions in both neuronal and glial populations. We generated *Nestin-Cre;CasL*$^{-/-}$*;Sin*$^{-/-}$
193 *;p130Cas*$^{fl/\Delta}$ (or more simply *Nes-Cre;TcKO*) mutants and started by confirming the specificity of
194 the p130Cas antibody by immunostaining control (*CasL*$^{-/-}$*;Sin*$^{-/-}$*;p130Cas*$^{fl/+}$) and littermate *Nes-*
195 *Cre;TcKO* brains at E16.5 (**Fig 1**; **S2 Fig**). The p130Cas antibody showed strong specificity for the
196 EC-AC tract and the cortical plate, with staining only remaining in *Nes-Cre;TcKO* animals in a
197 small subpopulation of cells in the hypothalamus (**S2 Fig**). We next performed
198 immunohistochemistry at P0 for the axon marker NCAM-L1 to examine the organization of
199 major cortical tracts (**Fig 3**). We observed notable disruptions to two major white matter tracts
200 in *Nes-Cre;TcKO* mutants: the Anterior Commissure (AC) and cortical white matter.

201 Axons of the External Capsule (EC) that, upon exit from the pallium, normally turn
202 medially to join the posterior Anterior Commissure (pAC), fail to fasciculate properly in *Nes-*
203 *Cre;TcKO* mutants, and instead project ventrally into the subpallium (**Fig 3A'** and **Fig 3B'**). Tracing
204 experiments using DiA crystals placed into the Somatosensory 2 (S2) region of the cortex (**S3C**
205 **Fig**) confirmed that these mis-projecting axons originate in the dorsolateral and lateral cortex
206 (**Fig 3C** and **Fig 3D**; n = 6 for *Nes-Cre;TcKO,* n = 7 for controls). We quantified axon pathfinding
207 errors by calculating the average number of stray pAC axon bundles per section per animal in
208 the subpallial area in *Nes-Cre;TcKO* mutants and control mice. The number of stray axon
209 fascicles in the subpallial area in *Nes-Cre;TcKO* animals averaged 4.23 ± 1.12, while the average
210 was 0 for control mice (**Fig 3I**; **S1 Table**; Unpaired *t*-test, p = 0.0004, n = 7 for *Nes-Cre;TcKO,* n =
211 10 for controls).

212 *Nes-Cre;TcKO* mutants also display severe defects in white matter within the cortical
213 plate, with large bundles of axons mis-projecting towards the pial surface (**Fig 3A''** and **Fig 3B''**).
214 We hereafter refer to these ectopic projections as Cortical Bundles (CBs). To quantify the CB
215 phenotype, we calculated the average number of CBs present per section per animal in the
216 cortex of both *Nes-Cre;TcKO* mutants and control mice. On average, we observed 7.88 ± 0.72
217 CBs in the cortex of *Nes-Cre;TcKO* and 0 in littermate controls (**Fig 3J**; **S1 Table**; Unpaired *t*-test,
218 $p < 0.0001$, n = 8 for *Nes-Cre;TcKO,* n = 7 for controls). The cortex receives input from multiple
219 cortical and subcortical areas, including contralateral connections via the corpus callosum and
220 AC [8] and thalamic connections from thalamocortical axon (TCA) projections [61,62]. We
221 therefore asked if the CB phenotype presented by *Nes-Cre;TcKO* mutants consisted of axons
222 originating from cortical or subcortical areas. Initial tracing experiments using DiA crystals
223 placed into the S2 cortex indicated that mis-projecting axons in CBs are not cortical in origin (**Fig**
224 **3E-F**). We performed additional lipophilic tracing experiments by placing DiI crystals into the
225 laterodorsal nucleus of the thalamus (**S3F Fig**) and found robust labeling of CBs in the ipsilateral
226 hemisphere in *Nes-Cre;TcKO* mutant neonates (**Fig 3E** and **Fig 3F**; n = 6 for *Nes-Cre;TcKO,* n = 5
227 for controls). This suggests that CBs form primarily from TCA afferents. Taken together, these
228 data point to a strong requirement for *Cas* family genes during cortical white matter tract
229 formation.

230 To examine the developmental progression of *Nes-Cre;TcKO* white matter tract defects,
231 we collected embryos at E14.6, E16.5, and E18.5 and performed immunohistochemistry for
232 NCAM-L1 (**Fig 4**). Interestingly, we observed different developmental trajectories for each
233 mutant phenotype. Initial formation of the EC-AC tract was unperturbed in *Nes-Cre;TcKO*

234 animals with no observable axon defasciculation at E14.5 (**Fig 4A'** and **Fig 4B'**; n = 4 for *Nes-*
235 *Cre;TcKO,* n = 4 for controls) and E16.5 (**Fig 4C'** and **Fig 4D'**; n = 8 for *Nes-Cre;TcKO,* n = 12 for
236 controls). It was not until late embryonic development (E18.5) that we detected aberrant axon
237 defasciculation in the AC (**Fig 4E'** and **Fig 4F'**, white arrowhead), with *Nes-Cre;TcKO* mutants
238 averaging 6.55 ± 1.09 stray axon bundles in the subpallial area, while control animals averaged 0
239 (**Fig 4G**; **S1 Table**; Unpaired *t*-test, p = 0.0011, n = 5 for *Nes-Cre;TcKO,* n = 4 for controls). In
240 contrast, the CB phenotype is apparent in *Nes-Cre;TcKO* mutants as early as E14.5 (**Fig 4A''** and
241 **Fig 4B''**, white asterisks), with the phenotype growing in severity as development continued (**Fig**
242 **4C''-F''**, white asterisks denote CBs). The average number of CBs in *Nes-Cre;TcKO* mutant mice
243 increased with age (4.29 ± 0.79 vs 5.06 ± 0.23 vs 9.06 ± 0.76), and at each embryonic time point,
244 the number of CBs observed on average in *Nes-Cre;TcKO* mutants was significantly higher
245 compared to littermate controls (**Fig 4H**; **S1 Table**; two-way ANOVA, p < 0.0001; Tukey honestly
246 significant difference (HSD) post hoc test, p < 0.0001 E14.5 *Nes-Cre;TcKO* versus control, E16.5
247 *Nes-Cre;TcKO* versus control, E18.5 *Nes-Cre;TcKO* versus control, E14.5 *Nes-Cre;TcKO* versus
248 E18.5 *Nes-Cre;TcKO*, E16.5 *Nes-Cre;TcKO* versus E18.5 *Nes-Cre;TcKO*; ns E14.5 *Nes-Cre;TcKO* vs
249 E16.5 *Nes-Cre;TcKO*; E14.5: n = 4 for *Nes-Cre;TcKO,* n = 4 for controls; E16.5: n = 8 for *Nes-*
250 *Cre;TcKO,* n = 12 for controls; E18.5: n = 5 for *Nes-Cre;TcKO,* n = 4 for controls). These results
251 suggest different developmental trajectories for each of the presented white matter tract
252 mutant phenotypes.

253 We next asked if *Cas* family genes are functioning in a cortical-autonomous and
254 neuronal-autonomous manner during establishment of the EC-AC and TCA tracts. With this aim,
255 we generated two new classes of *Cas TcKO* mutants by crossing TcKO animals into *Emx1-Cre* [63]

256 and *Nex-Cre* [64] driver lines. In contrast to the broad CNS expression of *Nestin-Cre*, *Emx1-Cre*
257 and *Nex-Cre* recombination events are largely restricted to the cortex, allowing us to assess for a
258 possible cortical-autonomous role of *Cas* genes. *Emx1-Cre* induces recombination in cortical
259 radial glial cells (RGCs), affecting RGCs, cortical excitatory neurons, and macroglial populations,
260 while *Nex-Cre* is active only in early postmitotic excitatory neurons within the cortex. By
261 comparing potential phenotypic differences between *Emx1-Cre;TcKO* and *Nex-Cre;TcKO* mutant
262 animals, we can evaluate if *Cas* genes function non-neuronal autonomously (i.e., in cortical non-
263 neuronal cells) or neuronal-autonomously (i.e., in cortical neurons) within the cortex (**S4 Fig**).

264 We have previously validated that *Emx1-Cre;TcKO* and *Nex-Cre;TcKO* mutant animals do
265 not produce functional *Cas* transcripts in the expected neural populations [43]. We then
266 generated *Emx1-Cre;CasL*$^{-/-}$*;Sin*$^{-/-}$ *;p130Cas*$^{fl/\Delta}$ (*Emx1-Cre;TcKO*) mutants and collected neonates
267 (P0) for immunohistochemistry using the axon marker NCAM-L1 (**Fig 5A-B''**). We observed
268 defasciculation of AC axons in *Emx1-Cre;TcKO* animals, which phenocopied the AC
269 defasciculation errors in *Nes-Cre;TcKO* neonates (**Fig 5A'** and **Fig 5B'**). These defasciculating AC
270 axons were labeled by lipophilic tracing from DiA crystals that were placed in the S2 region of
271 the cortex (**Fig 5C** and **Fig 5D**; n = 4 for *Emx1-Cre;TcKO,* n = 5 for controls). In *Emx1-Cre;TcKO*
272 mutants, we observed an average of 7.90 ± 1.43 stray axon bundles in the subpallial area, while
273 in control mice we observed 0 (**Fig 5M**; **S1 Table**; Unpaired *t*-test, p <0.0001, n = 8 for *Emx1-*
274 *Cre;TcKO,* n = 10 for controls). *Emx1-Cre;TcKO* animals also presented the ectopic CB phenotype,
275 with large bundles of axons mis-projecting to the pial surface (**Fig 5A''** and **Fig 5B''**). On average,
276 we observed 9.15 ± 0.43 CBs in *Emx1-Cre;TcKO* mice and 0 in controls (**Fig 5N**; **S1 Table**;
277 Unpaired *t*-test, p <0.0001, n = 8 for *Emx1-Cre;TcKO,* n = 10 for controls). Lastly, we performed

278 axon tracing experiments by placing DiI crystals into the thalamus of *Emx1;TcKO* neonates and
279 confirmed that these CBs are primarily formed by thalamic axons (**Fig 5E** and **Fig 5F**; n = 3 for
280 *Emx1-Cre;TcKO,* n = 3 for controls).

281 Our initial analysis showed that the CBs in *Nes-Cre;TcKO* mutants are primarily TCA
282 afferents originating from the thalamic nuclei (**Fig 3G** and **Fig 3H**). However, *Emx1-Cre* is not
283 expressed in the thalamic territory [63]. Thus, while the observation of CBs in *Emx1-Cre;TcKO*
284 mutants does not fully exclude the possibility of a thalamic role for Cas genes in TCA
285 innervation, it strongly suggests a cortical-autonomous role for Cas in guiding those axons,
286 thereby demonstrating that the white matter tract phenotypes in *Cas TcKO* animals require Cas
287 gene function in the developing neocortex itself.

288 Next, we generated *Nex-Cre;CasL*$^{-/-}$*;Sin*$^{-/-}$*;p130Cas*$^{fl/\Delta}$ (*Nex-Cre;TcKO*) mice and collected
289 neonates (P0) for immunohistochemistry using the axon marker NCAM-L1 (**Fig 5G-H''**). In
290 contrast to *Emx1-Cre;TcKO* mutants and *Nestin-Cre;TcKO* mutants, *Nex-Cre;TcKO* mutants only
291 presented the AC defasciculation phenotype (**Fig 5G'** and **Fig 5H'**, white arrowheads),
292 demonstrating a neuronal-autonomous role for *Cas* genes during AC fasciculation. These stray
293 AC axons were again confirmed to be dorsolateral and lateral in origin by lipophilic tracing from
294 DiA crystal placement into the S2 cortex (**Fig 5I** and **Fig 5J**, white arrowheads; n = 5 for *Nex-*
295 *Cre;TcKO,* n = 4 for controls). We observed an average of 8.47 ± 1.11 stray axon bundles in the
296 subpallial area of *Nex-Cre;TcKO* mutants and 0 in control mice (**Fig 5O**; **S1 Table**; Unpaired *t*-test,
297 $p < 0.0001$, n = 8 for *Nex-Cre;TcKO,* n = 7 for controls). Interestingly, *Nex-Cre;TcKO* mutant
298 neonates do not present the CB phenotype, indicating a non-neuronal autonomous role of *Cas*
299 genes in TCA projections (**Fig 5G''** and **Fig 5H''**; n = 8 for *Nex-Cre;TcKO,* n = 7 for controls).

300 Analyses of the three classes of *Cas TcKO* mutants thus indicate a complex requirement
301 for *Cas* genes during cortical white matter tract formation. The proper fasciculation of AC axons
302 appears to require *Cas* in a neuronal-autonomous manner, likely reflecting a requirement for
303 *Cas* genes in the projecting axons themselves. In contrast, the proper projection of TCA
304 afferents into the cortex appears to have a non-neuronal-autonomous requirement for *Cas*
305 genes. As such, we infer that *Cas* genes are required by some non-neuronal cortical cell
306 population to properly coordinate TCA guidance, possibly by controlling the positioning of
307 intermediate target populations or the provision of local guidance cues in the cortex.

308 To further assess the cortical- and neuronal-autonomous role of Cas genes during AC
309 fasciculation, we genetically labeled AC axons to confirm their cortical origins. This facilitated a
310 closer examination of their relationship to neighboring tracts. To this end, we made use of the
311 *Ai14/R26*$^{LSL\text{-}tdTomato}$ *Cre* reporter line (or simply *Ai14*), which expresses tdTomato fluorescent
312 protein upon Cre-mediated excision of upstream translational STOP sequences, permitting
313 visualization of cells or tissues that have or previously had Cre recombinase expression [65]. We
314 crossed the *Ai14* reporter line into the *Emx1-Cre;TcKO* line to generate *Emx1-Cre;Ai14*$^{+/-}$*;TcKO*
315 mutants and collected P0 neonates for immunohistochemistry with the marker NCAM-L1 (**Fig**
316 **6A-D''**). As expected, we found robust labeling of the EC-AC tract in *Emx1-Cre;Ai14*$^{+/-}$ controls
317 (*Emx1-Cre;Ai14*$^{+/-}$*;CasL*$^{+/-}$*;Sin*$^{+/-}$*;p130Cas*$^{+/+}$) and observed tight fasciculation of the AC tract in
318 these animals (**Fig 6A-B**). Examination of *Emx1-Cre;Ai14*$^{+/-}$*;TcKO* mutants revealed that 100% of
319 the large, defasciculating AC axon bundles were tdTomato+, genetically confirming the cortical
320 origin of these mis-projecting axons (**Fig 6D-D''**, white arrowheads). On average, we observed
321 9.5 ± 0.29 stray axon bundles in the subpallial area of *Emx1-Cre;Ai14*$^{+/-}$*;TcKO* mice and 0 in

322 *Emx1-Cre;Ai14*$^{+/-}$ controls (**Fig 6I**; **S1 Table**; Unpaired *t*-test p < 0.0001, n = 3 for *Emx1-Cre;Ai14*$^{+/-}$
323 *;TcKO*, n = 3 for controls). Interestingly, we also observed tdTomato-/NCAM-L1+ processes that
324 diffusely populated the subpallium. The thicker bundles of tdTomato+/NCAM-L1+ processes
325 appeared to intercalate with these tdTomato-/NCAM-L1+ processes (**Fig 6D**), suggesting that
326 Cas-deficient tdTomato+ axons might be improperly associating with other axonal processes.

327 We next crossed the *Ai14* reporter line into the *Nex-Cre;TcKO* line to generate
328 *NexCre;Ai14*$^{+/-}$*;TcKO* mutants and collected P0 neonates for immunohistochemistry with the
329 marker NCAM-L1 (**Fig 6E-H''**). As observed with *Emx1-Cre;Ai14*$^{+/-}$ controls, we found robust
330 labeling of the EC-AC tract in *Nex-Cre;Ai14*$^{+/-}$ controls (*Nex-Cre;Ai14*$^{+/-}$*;CasL*$^{+/-}$*;Sin*$^{+/-}$*;p130Cas*$^{+/+}$)
331 (**Fig 6E-F**). In *Nex-Cre;Ai14*$^{+/-}$*;TcKO* mutants, we observed large, defasciculating AC axon bundles
332 in the subpallial area, 100% of which were tdTomato+ (**Fig 6H-H''**, white arrowheads). On
333 average, we observed 9.33 ± 2.03 stray axon bundles in the subpallial area in *Nex-Cre;Ai14*$^{+/-}$
334 *;TcKO,* while in *Nex-Cre;Ai14*$^{+/-}$ controls, we observed 0 (**Fig 6J**; **S1 Table**; Unpaired *t*-test p =
335 0.0116, n = 4 for *Nex-Cre;Ai14*$^{+/-}$*;TcKO,* n = 3 for controls). As in *Emx1-Cre;Ai14*$^{+/-}$*;TcKO* mutants,
336 the defasciculating tdTomato+/NCAM-L1+ AC processes in *Nex-Cre;Ai14*$^{+/-}$*;TcKO* mutants
337 appeared to intercalate with the tdTomato-/NCAM-L1+ bundles that also populate the
338 subpallium (**Fig 6H**). Taken together, these data genetically confirm the cortical origins of
339 defasciculating axons in the AC while also supporting the neuronal-autonomous role of *Cas*
340 genes for proper AC fasciculation.

341 During canonical adhesion signaling events, Cas proteins are recruited to early Integrin
342 Adhesion Complexes (IACs) via β1-integrin receptor stimulation and subsequent activation of
343 the non-receptor tyrosine kinases Focal Adhesion Kinase (FAK) and Src [34]. In the mammalian

344 brain, β1-integrin, encoded by *Itgb1*, appears to be the most prevalent β subunit involved in
345 mediating adhesion signaling events [66–70], with established roles in axonal guidance and
346 growth cone dynamics [67,71–73]. It has been demonstrated that *Itgb1* is expressed in the
347 developing cortex [74,75]. We attempted to validate β1-integrin protein expression in the
348 developing cortex using two different β1-integrin antibodies, but neither demonstrated
349 specificity (**S5-S6 Figs**). To investigate whether β1-integrin could be the adhesion receptor acting
350 upstream of Cas proteins during cortical white matter tract development, we asked if the
351 requirement for *Cas* genes in AC fasciculation and TCA projection was also observed in *Itgb1*
352 mutants.

353 We therefore generated *Emx1-Cre;Itgb1*$^{fl/fl}$ and *Nex-Cre;Itgb1*$^{fl/fl}$ mice and performed
354 immunohistochemistry in neonates (P0) using the axon marker NCAM-L1 (**Fig 7**). We first
355 examined the AC commissure tract in *Emx1-Cre;Itgb1*$^{fl/fl}$ and *Nex-Cre;Itgb1*$^{fl/fl}$ neonates.
356 Remarkably, neither class of *Itgb1* mutants phenocopied the AC defasciculation defects
357 observed in *Cas TcKO* mutants (**Fig 7A', Fig 7B', Fig 7C',** and **Fig 7D'**; n = 6 for *Emx1-Cre;Itgb1*$^{fl/fl}$, n
358 = 5 for controls; n = 3 for *Nex-Cre;Itgb1*$^{fl/fl}$ mutants, n = 4 for controls). These observations
359 demonstrate that the β1-integrin receptor by itself is dispensable for AC fasciculation,
360 suggesting a different receptor may be acting upstream of *Cas* genes during AC formation. We
361 next examined the cortices of *Emx1-Cre;Itgb1*$^{fl/fl}$ and *Nex-Cre;Itgb1*$^{fl/fl}$ mutants and observed
362 bundles of mis-projecting axons in *Emx1-Cre;Itgb1*$^{fl/fl}$ mutants, a defect that strongly
363 phenocopied the CB phenotype presented by *Emx1-Cre;TcKO* mutants (**Fig 7A''** and **Fig 7B''**,
364 white asterisks). On average, we observed 8.08 ± 0.25 CBs in *Emx1-Cre;Itgb1*$^{fl/fl}$ animals and 0 in
365 controls (**Fig 7E**; **S1 Table**; Unpaired *t*-test, $p < 0.0001$, n = 6 for *Emx1-Cre;Itgb1*$^{fl/fl}$, n = 5 for

366 controls). Interestingly, *Nex-Cre;Itgb1*$^{fl/fl}$ mutants did not display Cortical Bundles (**Fig 7C''** and
367 **Fig 7D''**; n = 3 for *Nex-Cre;Itgb1*$^{fl/fl}$ mutants, n = 4 for controls). This suggests similar non-
368 neuronal-autonomous roles for β1-integrin and Cas proteins during TCA projection pathfinding.

369 Given that β1-integrin seems to be dispensable on its own for AC formation, we sought
370 to determine the expression of other β-integrin subunits previously reported to be expressed
371 during cortical development [75]. Transcripts for the β-integrin subunits β5-, β6-, and β8-
372 integrin (encoded by *Itgb5*, *Itgb6*, and *Itgb8*, respectively) are indeed expressed in the
373 developing neocortex at E14.5 (**S7 Fig**), E16.5 (**S8 Fig**), and E18.5 (**S9 Fig**), with overlapping
374 expression in the ventricular zone at E18.5 (**S9 Fig**). Moreover, throughout development, *Itgb6*
375 and *Itgb8* are diffusely expressed in the piriform cortex (**S7-S9 Figs**), where neurons that project
376 axons that contribute to the formation of the pAC reside.

377 Lastly, we sought to identify a developmental mechanism by which TCA afferents mis-
378 project to form CBs in *Cas TcKO* mutants. Previous research from our lab established a role for
379 Cas proteins and β1-integrin during cortical lamination [43]. We therefore asked if the CB
380 phenotype presented by *Emx1-Cre;TcKO* and *Emx1-Cre;Itgb1*$^{fl/fl}$ mutants was a secondary
381 phenotype that resulted from the disruption of cortical lamination in these mutants. As
382 previously mentioned, the subplate is a transient structure that acts as an intermediate target
383 for TCAs, coordinating the entry of these thalamic axons into the cortical plate [22,61]. Given
384 the cortical requirement of *Cas* genes for TCA guidance, and the defects in cortical lamination
385 presented by *Cas TcKO* mutants [43], we hypothesized that one possible explanation for the CB
386 phenotype presented by our mutants here could be the displacement of subplate and other
387 deep-layer neurons in *Emx1-Cre;TcKO* and *Emx1-Cre;Itgb1*$^{fl/fl}$ mutants.

388 Thus, we performed immunohistochemistry in *Emx1-Cre;TcKO* and *Emx1-Cre;Itgb1*$^{fl/fl}$

389 mutants at E16.5 (**Fig 8**) and P0 (**Fig 9**), using the markers NCAM-L1 and Tbr1. Tbr1 is a

390 transcription factor known to regulate the specification of the subplate and layer VI cortical

391 layers [76]. Indeed, we found, at E16.5 and P0, both *Emx1-Cre;TcKO* and *Emx1- Cre;Itgb1*$^{fl/fl}$

392 mutants displayed cortical dysplasia, as previously described [43]: lamination of deep-layer

393 Tbr1+ cells is highly disrupted, with columns of Tbr1+ cells reaching the marginal zone (**Fig 8B**

394 and **Fig 8D**, **Fig 8F** and **Fig 8H**; **Fig 9B** and **Fig 9D**, **Fig 9F** and **Fig 9H**). Interestingly, in both *Emx1-*

395 *Cre;TcKO* and *Emx1-Cre;Itgb1*$^{fl/fl}$ mutants, 100% of the NCAM-L1+ CBs associated with these

396 displaced Tbr1+ cells, at times with clear "tunnels" of Tbr1+ cells containing CBs invading the

397 marginal zone (**Fig 8D-D''** and **Fig 8H-H''**, white asterisks; **Fig 9D-D''** and **Fig 9H-H''**, white

398 asterisks; n = 5-8 per group, see figure legends for details). We have previously demonstrated

399 that there are no cortical lamination defects in P7 *Nex-Cre;TcKO* and *Nex-Cre;Itgb1*$^{fl/fl}$ mutants

400 [43]. Additional analysis of *Nex-Cre;TcKO* animals at P0, using the markers NCAM-L1 and Tbr1,

401 showed no apparent differences in cortical lamination between *Nex-Cre;TcKO* mutants and

402 littermate controls (n = 4 for *Nex-Cre;TcKO* mutants, n = 4 for controls) (**S10 Fig**). Taken together,

403 these results demonstrate that the disorganization of the subplate and deep cortical layers

404 observed in pan-cortical *Cas TcKO* and *Itgb1* mutant mice is non-neuronal autonomous and

405 strongly correlates with the ectopic CB phenotype.

406

407 **Discussion**

408 In this study, we used conditional mouse genetics to assess the cortical-autonomous and
409 neuronal-autonomous roles of *Cas* genes during forebrain white matter tract formation. Using a
410 *Cas* triple conditional knockout (*Cas TcKO*) model, we provide strong genetic evidence that Cas
411 proteins are required in two manners: 1) cortical- and neuronal-autonomously for proper
412 fasciculation of the posterior branch of the Anterior Commissure (pAC) (**Fig 3B'** and **Fig 3D**), and
413 2) cortical- and non-neuronal autonomously for thalamocortical axon (TCA) guidance (**Fig 3B''**
414 and **Fig 3H**).

415 The AC is a highly evolutionarily conserved forebrain tract that, in mice, makes reciprocal
416 connections between the Anterior Olfactory Nuclei of each olfactory bulb (via the anterior AC
417 tract, aAC) and mediates reciprocal connections between the piriform and entorhinal cortices of
418 the two hemispheres (via the posterior AC tract, pAC) [32]. Recent developmental studies have
419 identified a small group of pioneering axons with unusual elongation kinetics that advance
420 towards the embryonic midline at E13, preceding the majority of pAC axons that arrive later at
421 E15 [33]. These late-arriving processes join the stalled pioneers to form a primary fascicle that
422 crosses the embryonic midline in unison at E16 then innervates contralaterally and achieves
423 specific target selection at E17 and E18, respectively [33]. In our study, we find that *Cas TcKO*
424 mutants display defasciculation and ventral targeting of axons of the pAC tract (**Fig 3B'** and **Fig**
425 **3D**). However, these defects are only observable at later embryonic (E18.5) and postnatal (P0)
426 stages (**Fig 4F** and **Fig 3B**). Considering the timeline of pAC formation, this suggests that the
427 axons that fail to fasciculate properly are a population of late "follower" axons arriving at the AC
428 later in development.

429 Interestingly, we find that the defasciculating AC processes originate from the
430 dorsolateral cortex, as they are labeled by lipophilic tracing from the somatosensory S2 cortex in
431 all three classes of *Cas TcKO* mutants analyzed (**Fig 3D**; **Fig 5D** and **Fig 5J**). These results are
432 somewhat unexpected: the pAC has been primarily described as carrying axons from
433 ventrolateral cortical areas in mice [32]. The observation of DiI-labeled AC axons in both control
434 and mutant animals after placement of dye crystals in S2 might suggest that a population of
435 cortical axons projecting along the EC contributes to the formation of the AC. However, we
436 cannot exclude the possibility that DiI cross-labeled other AC-projecting cortical axons ventral to
437 S2. We genetically confirmed the cortical origin of the defasciculating AC axons using the *Ai14*
438 *Cre*-dependent reporter in both the *Emx1-Cre* and *Nex-Cre* lines (**Fig 6**). Additionally, we
439 observed intercalation of defasciculating tdTomato+ AC processes with other tdTomato-/NCAM-
440 L1+ processes in the subpallium. This may suggest that these defasciculating axons may be
441 failing to properly regulate homotypic versus heterotypic associations [77]. Taken together,
442 these data support a neuronal-autonomous requirement of *Cas* genes for the guidance of a
443 subset of cortical axons, which in the absence of these genes, mis-project into the ventral
444 subpallium.

445 During canonical adhesion signaling, Cas proteins are recruited to Integrin Adhesion
446 Complexes (IACs) following integrin receptor activation [34,39,78]. The integrins are a large
447 family of transmembrane receptors that include 18 alpha (α) and 8 beta (β) subunits and are
448 known to form 24 combinations of αβ heterodimers [79,80]. The β1-integrin subunit has been
449 particularly well studied and is found in 12 of the known heterodimer combinations, mediating
450 many intracellular signaling functions during CNS development [42,66–69,75,80,81]. We

451 therefore analyzed the structure of the AC in *Itgb1* mutant neonates, which are deficient for the
452 β1-integirn subunit. Surprisingly, conditional deletion of *Itgb1* using *Emx1-Cre* or *Nex-Cre* failed
453 to phenocopy the AC defasciculation defects observed in *Cas TcKO* mutants (**Fig 7**), suggesting
454 that β1-integrin is dispensable for proper fasciculation of this tract. This raises two intriguing
455 possibilities: 1) there is compensation by another β subunit in *Itgb1*-deficient mice, or 2) Cas
456 proteins are signaling downstream of a different type of receptor.

457 In support of the first possibility, β5-integrin, β6-integrin, and β8-integrin are expressed
458 in the embryonic cortex (**S7-S9 Figs**) [75]. Thus, they might be acting as part of the adhesion
459 receptors driving the fasciculation of the AC axons, or might compensate for the loss of *Itgb1* in
460 mutant mice via the formation of heterodimers with α-integrins. For example, heterodimer
461 formation between αV-integrin and β1-, β5-, β6-, and β8-integrin has been previously
462 documented [80]. Of all α-subunits, αV-integrin appears as a prime candidate to modulate this
463 process: in addition to being able to form heterodimers with multiple β-integrins, αV-integrin is
464 known to have a critical role in neurodevelopment and is expressed in axons of white matter
465 tracts in the cerebral cortex [82,83]. Moreover, αV-integrin-containing dimers bind to the ECM
466 molecules laminin, fibronectin, vitronectin, tenascin, and collagen [68,75]. Importantly, laminin,
467 fibronectin, and tenascin are expressed by a population of midline glial cells that help
468 coordinate the development of the pAC [29]. One possible scenario then is that β5-integrin, β6-
469 integrin, or β8-integrin is acting as a functional partner with αV-integrin during AC fasciculation,
470 or can at least compensate for the loss of *Itgb1.*

471 The second possible explanation for the failure of *Itgb1* mutants to phenocopy the AC
472 defasciculation defects presented by *Cas TcKO* animals is that Cas proteins are signaling

473 downstream of an entirely different receptor system. It has previously been shown that
474 phospho-activation of Cas can be modulated by CXCL12/CXCR4 [44], Neuropilin [45], Netrin
475 [46], and Eph/Ephrin [84] signaling. Moreover, mutations in several genes that participate in
476 these signaling pathways or have known roles in adhesion have been shown to affect the
477 development of the AC; however, most of these mutations result in thinning or absence of the
478 AC tracts, not defasciculation of AC axons [85–107].

479 Notably, *Ephb2/Nuk* mutants [86] and *Ephb1/Ephb2* double-mutants [87] display
480 defasciculation and ventral targeting of pAC axons, which partially phenocopy *Cas TcKO*
481 mutants. Moreover, biochemical studies have implicated cross-talk between β1-integrin and
482 EphB/EphrinB receptor pathways in various cell types [108–111], including retinal ganglion cells
483 [112] and mossy fiber axons [113]. It is possible that these signaling cascades may be
484 coordinating phosphorylation of Cas proteins in cortical neuron axons as well. Determining
485 whether Cas proteins are working downstream of Eph/Ephrin receptor systems during AC
486 projection and fasciculation will be an interesting goal for future studies.

487 The second white matter tract phenotype presented by *Cas TcKO* mutants is the
488 appearance of large ectopic bundles of axons mis-projecting towards the pial surface of the
489 cortex (**Fig 3A''** and **Fig 3B''**), which we termed Cortical Bundles (CBs). Lipophilic tracing
490 experiments revealed the origin of these mis-projections to be thalamic (**Fig 3F** and **Fig 3H**).
491 Analysis of cortical bundle formation in *Emx1-Cre;TcKO* revealed a comparable phenotype to
492 that observed in *Nestin-Cre;TcKO*, strongly suggesting a cortical-autonomous role for *Cas* genes
493 in CB formation. Further genetic experiments demonstrated that this phenotype is non-
494 neuronal-autonomous: conditional deletion of *Cas* genes using *Nex-Cre* failed to recapitulate

495 the CB phenotype (**Fig 5H''** and **Fig 5L**). From this, we inferred that *Cas* gene function is required
496 by some non-neuronal cortical-resident population responsible for coordinating TCA entry.
497 Similarly, analysis of *Itgb1* mutants revealed that conditional deletion using *Nex-Cre* did not
498 result in CB formation (**Fig 7D''**), indicating a comparable cortical-autonomous, non-neuronal-
499 autonomous role for β1-integrin. However, we cannot formally exclude a thalamus-autonomous
500 role for *Itgb1* or *Cas* genes in TCA pathfinding, as we did not ablate these genes exclusively in
501 the thalamus. Future studies using thalamus-specific Cre drivers would be needed to definitively
502 address this question.

503 During normal development, TCA innervation of the cortex is regulated by a transient
504 structure known as the subplate which acts as an intermediate target for TCAs until their target
505 layer (layer IV) is fully formed [15]. Arriving TCA projections stall in the subplate for several days
506 and grow extensive side processes within the subplate during this waiting period [18–20]. Upon
507 entering the cortical plate, TCAs form transient microcircuits with subplate neurons and
508 maturing cortical layer IV neurons, a process which appears to facilitate the proper targeting of
509 layer IV and thus the organization of mature circuits [23,114,115]. Mutations that disrupt the
510 laminar organization of the subplate, such as *reeler* mutants [116] and *Cdk5* mutants [117],
511 result in aberrant TCA projection patterns within the cortical plate, speaking to the
512 developmental importance of the subplate in TCA guidance. Previous work from our lab and
513 other labs has demonstrated that *Cas TcKO* and *Itgb1* mutants have severely disrupted laminar
514 organization of the cortex caused by breakages in the basal lamina that destabilize radial glial
515 endfeet attachment, thus resulting in improper migration of cortical neurons and severe cortical
516 dysplasia [43,74,118].

517 Taking all of this into consideration, we asked whether the disruption of subplate and
518 layer VI organization observed in *Cas TcKO* and *Itgb1* mutants could be a contributing
519 developmental factor to the cortical-autonomous defects we observed in TCA guidance. Using
520 the subplate/Layer VI marker Tbr1, we observed severe displacement of the deep cortical layers
521 at E16.5 (**Fig 8**) and P0 (**Fig 9**) in both *Cas TcKO* and *Itgb1* mutants. Co-labeling with NCAM-L1
522 revealed that 100% of ectopic CB projections correlate with sites of displaced Tbr1+ cells (**Fig 8D**
523 and **Fig 8H**; **Fig 9D** and **Fig 9H**).

524 Within the context of our previous work [43], these results suggest a model
525 whereby *Cas* genes are required in cortical radial glial cells to regulate endfeet attachment,
526 stabilization of the basement membrane, and glial process organization, which subsequently aid
527 in neuronal migration and formation of the cortical layers, including the subplate. In the
528 absence of *Cas* or *Itgb1* genes, these radial glial tracks are disrupted, resulting in mispositioned
529 subplate neurons (**Fig 8D** and **Fig 8H**; **Fig 9D** and **Fig 9H**) [43]. These mispositioned subplate
530 neurons could potentially recruit TCAs for innervation, causing ectopic cortical bundles to
531 innervate the proper intermediate target positioned in the wrong location. Hence, our model
532 (**S4 Fig**) is that while the role of *Cas* genes is non-neuronal-autonomous (acting in radial glia
533 rather than in the neurons themselves), the mispositioned Tbr1+ neurons in *Emx1-*
534 *Cre;TcKO* mutants drive the TCA misprojection phenotype. These results, however indirect, add
535 to an extensive body of literature suggesting that proper lamination and formation of the
536 subplate is required for appropriate TCA afferent projection [15–19,21–23,61,119–124].

537 Collectively, this work establishes Cas proteins as essential mediators of forebrain axon
538 tract development and provides genetic mechanistic insights into their cell-type-specific

539 functions during cortical lamination-dependent thalamocortical guidance and neuronal-
540 autonomous commissural fasciculation. We build on previous genetic evidence that *Cas* genes
541 function radial glial-autonomously downstream of the β1-integrin receptor to ensure proper
542 lamination of the cortex [43], demonstrating that errors in lamination result in disruptions to
543 the subplate. Based on our data, we propose that this misplacement of the subplate might
544 cause aberrant thalamocortical axon guidance and the formation of ectopic bundles that mis-
545 project towards the pial surface. Further, we provide genetic evidence that *Cas* genes function
546 independently of the β1-integrin receptor in a neuronal-autonomous manner during
547 fasciculation and guidance of the Anterior Commissure, demonstrating that a subset of late-
548 arriving axons fail to properly fasciculate with the posterior branch of the Anterior Commissure.
549 These defasciculating axons display improper ventral targeting upon crossing the pallial-
550 subpallial boundary (PSPB). Our findings add to a growing body of evidence suggesting essential
551 roles for Cas proteins in adhesion signaling during axon guidance and migration [34,41–
552 43,46,52,125,126].

553

554 **Materials & Methods**

555 **Animals and Genotyping:** For embryonic collections, the morning of vaginal plug observation
556 was designated as embryonic day 0.5 (E0.5) and the day of birth was postnatal day 0 (P0). The
557 generation of the *Cas TcKO* model has been previously described [42,127,128]. Swiss Webster
558 mice were purchased from Taconic Biosciences (Model: SW-F and SW-M). The following lines
559 were purchased from The Jackson Laboratory: *Nestin-Cre* (Stock: 003771), *Emx1-Cre* (Stock:

560 005628), *Ai14/R26*$^{LSL\text{-}tdTomato}$ (Stock: 007914), and *Itgb1*$^{fl/fl}$ (Stock: 004605). Genotyping for
561 *Nestin-Cre* was carried out using the following primers: F: CCT TCC TGA AGC AGT AGA GCA R:
562 GCC TTA TTG TGG AAG GAC TG. Genotyping for *Emx1-Cre* was carried out using the following
563 primers: F: CCA TAT CAA CCG GTG GCG CAT C and R: TCG ATA AGC TTG GAT CCG GAG AG.
564 Genotyping for *Ai14/R26*$^{LSL\text{-}tdTomato}$ was carried out using the following primers: WTF: AAG GGA
565 GCT GCA GTG GAG TA, WTR: CCG AAA ATC TGT GGG AAG TC, MutF: CTG TTC CTG TAC GGC ATG
566 G, and MutR: GGC ATT AAA GCA GCG TAT CC. Genotyping for *Itgb1*$^{fl/fl}$ mice was carried out using
567 the primers: F: CGG CTC AAA GCA GAG TGT CAG TC and R: CCA CAA CTT TCC CAG TTA GCT CTC.
568 *Nex-Cre* mice were kindly provided by Drs. Nave and Goebbels [64,129]. Genotyping for *Nex-Cre*
569 was carried out using the following primers: Primer 4: GAG TCC TGG AAT CAG TCT TTT TC,
570 Primer 5: AGA ATG TGG AGT AGG GTG AC, and Primer 6: CCG CAT AAC CAG TGA AAC AG. Tail
571 biopsies were digested with Quanta tail extraction reagent kit (cat: 95091-025). PCR reactions
572 were prepared using GoTaq Master Mix (Promega cat: PRM7123). All animal procedures were
573 performed according to the University of California, Riverside's Institutional Animal Care and
574 Use Committee (IACUC) guidelines. All procedures were approved by UC Riverside IACUC.

575 **Immunohistochemistry:** Embryos, neonates, and adult mice were transcardially perfused with
576 ice-cold 1xPBS and subsequently dissected in cold 1xPBS. Brain tissue was post-fixed in 4% PFA
577 (diluted in 1xPBS) for 2hrs – overnight at 4°C. Tissue samples were processed immediately as
578 floating sections or cryopreserved in a solution of 30% sucrose in 1xPBS before embedding in
579 Tissue Plus O.C.T. Compound (Fisher HealthCare, cat: 4585) for long-term storage. Tissue
580 processed as floating sections was embedded in 3% agarose and sectioned coronally as 100-
581 150µm sections on a vibratome (Lecia, cat: VT1000S). Floating sections were incubated with a

582 permeabilization solution containing 3% bovine serum albumin (BSA) and 0.3% TritonX-100 in
583 1xPBS for 4hrs – overnight at 4°C. Primary and secondary antibody mixes were diluted in a
584 solution of 5% goat serum made with permeabilization solution. All antibody incubations were
585 overnight at 4°C with gentle agitation. Cryoprotected samples were sectioned coronally at 25-
586 50µm on a cryostat (Leica cat: CM3050). Cryosections were dried for 20 minutes at room
587 temperature before blocking in freshly prepared blocking buffer (10% goat serum and 0.1%
588 TritonX-100 in 1xPBS) for 1hr before primary antibody addition. Antibodies were then prepared
589 in blocking buffer with reduced goat serum (5%) and incubated in a humidified chamber
590 overnight at 4°C. The antibodies and concentrations used in this study: rabbit anti-p130Cas
591 (E1L9H) (1:200, Cell Signaling Technology cat: 13846), rat anti-NCAM-L1 (1:500, Millipore cat:
592 MAB5272), chicken anti-Nestin (1:500, Aves cat: NES), chicken anti-GFP (1:500, Aves cat: GFP-
593 1020), rabbit anti-dsRed (1:500, Takara Bioscience cat: 632496), rabbit anti-Tbr1 (1:500, Abcam
594 cat: ab31940 [polyclonal]), rabbit anti-Tbr1 (1:500, Abcam cat: ab183032 [monoclonal]), mouse
595 anti-CD29 (Integrin beta 1) (1:100, eBioscience cat: 14-0299-82), and rabbit anti-Integrin β1
596 (D6S1W) (1:100, Cell Signaling Technology cat: 34971). Secondary antibodies were purchased
597 from ThermoFisher and diluted to 1:1000 from the stock concentration: goat anti-chicken 488
598 (cat: A-11039), goat anti-chicken 546 (cat: A-11040), goat anti-rabbit 488 (cat: A-11034), goat
599 anti-rabbit 546 (cat: A-11035), goat anti-rabbit 647 (cat: A-21244), goat anti-rat 488 (cat: A-
600 21208), goat anti-rat 546 (cat: A-11081), and goat anti-mouse 647 (cat: A-21236). Nuclear
601 counterstain was achieved by co-incubation with 1ug/ml DAPI (ThermoFisher cat: 50850585) in
602 all secondary antibody incubations. Tissue was mounted using Fluoro Gel with DABCO (Electron
603 Microscopy Sciences, cat: 17985-02). Confocal scanning images were acquired on a Leica DMi8

604 using a 10x objective (NA=0.40) or 20x objective (NA=0.75), and z-stacks were acquired with 20-
605 40 steps of sizes of 2-4µm.

606 **Fluorescent *in situ* Hybridization:** Embryos were perfused and dissected as described above for
607 immunohistochemistry. Brain tissue was then post-fixed in 4% PFA (in 1xPBS) overnight at 4°C
608 and cryopreserved as previously described. Fluorescent *in situ* hybridization was performed on
609 20 µm cryosections from E14.5, E16.5, or E18.5 embryos using the RNAScope Multiplex
610 Fluorescent Detection Kit v2 from Advanced Cell Diagnostics according to the manufacturer's
611 instructions (ACD, 323110) [130]. Briefly, ssDNA "z-probes" hybridize complementary to the
612 RNA of interest. Oligos bind to the tail region of the z-probe and are bound to amplifiers labeled
613 with horseradish peroxidase (HRP) and fluorophores. *Itgb5* (ACD, 404311), *Itgb6* (ACD, 312501),
614 and *Itgb8* (ACD, 407931) probes generated by Advanced Cell Diagnostics were uniquely
615 amplified with Opal dyes (Akoya Biosciences, FP1487001KT, FP1488001KT, FP1496001KT) and
616 counterstained with DAPI (1 µg/ml). Slides were mounted using Fluoro Gel with DABCO.
617 Confocal scanning images were acquired on a Leica DMi8.

618 **Axonal Tracing:** Lipophilic tracing of white matter tracts was performed by manually placing
619 small crystals of either DiA (Invitrogen cat: D3883) or DiI (Invitrogen cat: D282) into neonate
620 tissue dissected as described above for immunohistochemistry and postfixed in 4% PFA (in
621 1xPBS) overnight at 4°C. DiA crystals were placed in the Somatosensory 2 (S2) region of the
622 cortex, while DiI crystals were placed in the laterodorsal thalamus. Lipophilic crystals were
623 allowed to diffuse for 8 weeks at 37°C in a solution of 4% PFA in 1xPBS, with the solution
624 changed daily for the first 4 days and weekly thereafter. Tissue was embedded in 3% agarose in

625 1xPBS and sectioned as 150 µm sections on a vibratome (Lecia, cat: VT1000S). Sections were
626 imaged freshly sliced on a Zeiss Axio Imager 2 microscope.

627 **Quantification of Stray Axon Bundles and Cortical Bundles:** Quantification of stray axon
628 bundles defasciculating from the EC-AC tract and mis-projecting Cortical Bundles (CBs) was
629 done using ImageJ. The number of stray axon bundles in the subpallial area and the number of
630 CBs in the cortex were counted manually for each section per animal using the ImageJ
631 multipoint tool. Three to twelve independent animals were analyzed per group, depending on
632 the experiment, and two to twelve sections were analyzed per animal. Bar graphs represent the
633 group mean ± standard error of group mean, with plotted values representing the mean from
634 each animal analyzed. The datasets were then tested for normality using the Shapiro–Wilk test
635 and QQ plot. For normally distributed datasets, Unpaired *t*-test was performed for comparing
636 two independent samples and two-way ANOVA, followed by Tukey honestly significant
637 difference (HSD) post hoc test, was used for multiple comparisons.

638 **Ethics approval:** All animal procedures presented here were performed according to the
639 University of California, Riverside's Institutional Animal Care and Use Committee (IACUC)-
640 approved guidelines, under protocol A-8.

641 **Acknowledgements**

642 We would like to thank Dr. Teresa Ubina for critically reading the manuscript and providing
643 helpful comments. We would like to thank Drs. Nave and Goebbels for the *Nex-Cre* mice. We
644 would also like to thank Drs. Sachiko Seo and Mineo Kurokawa, and Dr. Konstantina
645 Alexandropoulos for sharing the *CasL*$^{-/-}$ and *Sin*$^{-/-}$ mouse lines, respectively.

646 **Competing interests**

647 The authors declare no competing financial interests.

648 **Availability of data and materials**

649 All data analyzed during this study are included in this article and supporting files.

650 **Authors Contributions**

651 JAE and AMT designed and performed experiments and wrote the manuscript. PAR, PW, and
652 WW designed and performed experiments. MMR conceived the project, designed experiments,
653 and wrote the manuscript.

654 **References**

655 1. Tessier-Lavigne M, Goodman CS. The molecular biology of axon guidance. Science
656 1996;274:1123–33.

657 2. Kolodkin AL, Tessier-Lavigne M. Mechanisms and molecules of neuronal wiring: a primer. Cold
658 Spring Harb Perspect Biol 2011;3:a001727.

659 3. Caudy M, Bentley D. Pioneer growth cone steering along a series of neuronal and non-neuronal
660 cues of different affinities. J Neurosci 1986;6:1781–95.

661 4. Lefcort F, Bentley D. Pathfinding by pioneer neurons in isolated, opened and mesoderm-free limb
662 buds of embryonic grasshoppers. Dev Biol 1987;119:466–80.

663 5. Easter SS, Ross LS, Frankfurter A. Initial tract formation in the mouse brain. J Neurosci
664 1993;13:285–99.

665 6. Easter SS, Burrill J, Marcus RC, Ross LS, Taylor JS, Wilson SW. Initial tract formation in the
666 vertebrate brain. Prog Brain Res 1994;102:79–93.

667 7. Wang L, Marquardt T. What axons tell each other: axon-axon signaling in nerve and circuit
668 assembly. Curr Opin Neurobiol 2013;23:974–82.

669 8. Chédotal A, Richards LJ. Wiring the brain: the biology of neuronal guidance. Cold Spring Harb
670 Perspect Biol 2010;2:a001917.

671 9. Moreland T, Poulain FE. To Stick or Not to Stick: The Multiple Roles of Cell Adhesion Molecules in
672 Neural Circuit Assembly. Front Neurosci 2022;16:889155.

673 10. Breau MA, Trembleau A. Chemical and mechanical control of axon fasciculation and
674 defasciculation. Semin Cell Dev Biol 2023;140:72–81.

675 11. López-Bendito G, Cautinat A, Sánchez JA, Bielle F, Flames N, Garratt AN, et al. Tangential neuronal
676 migration controls axon guidance: a role for neuregulin-1 in thalamocortical axon navigation. Cell
677 2006;125:127–42.

678 12. Garel S, López-Bendito G. Inputs from the thalamocortical system on axon pathfinding
679 mechanisms. Curr Opin Neurobiol 2014;27:143–50.

680 13. Squarzoni P, Thion MS, Garel S. Neuronal and microglial regulators of cortical wiring: usual and
681 novel guideposts. Front Neurosci 2015;9:248.

682 14. Vanderhaeghen P, Polleux F. Developmental mechanisms patterning thalamocortical projections:
683 intrinsic, extrinsic and in between. Trends Neurosci 2004;27:384–91.

684 15. Molnár Z, Garel S, López-Bendito G, Maness P, Price DJ. Mechanisms controlling the guidance of
685 thalamocortical axons through the embryonic forebrain. Eur J Neurosci 2012;35:1573–85.

686 16. López-Bendito G. Development of the Thalamocortical Interactions: Past, Present and Future.
687 Neuroscience 2018;385:67–74.

688 17. Molnár Z, Kwan KY. Development and Evolution of Thalamocortical Connectivity. Cold Spring Harb
689 Perspect Biol 2024;16:a041503.

690 18. Ghosh A, Antonini A, McConnell SK, Shatz CJ. Requirement for subplate neurons in the formation
691 of thalamocortical connections. Nature 1990;347:179–81.

692 19. Allendoerfer KL, Shatz CJ. The subplate, a transient neocortical structure: its role in the
693 development of connections between thalamus and cortex. Annu Rev Neurosci 1994;17:185–218.

694 20. Ayoub AE, Kostovic I. New horizons for the subplate zone and its pioneering neurons. Cereb
695 Cortex 2009;19:1705–7.

696 21. McConnell SK, Ghosh A, Shatz CJ. Subplate neurons pioneer the first axon pathway from the
697 cerebral cortex. Science 1989;245:978–82.

698 22. Ghosh A, Shatz CJ. Involvement of subplate neurons in the formation of ocular dominance
699 columns. Science 1992;255:1441–3.

700 23. Kanold PO, Luhmann HJ. The subplate and early cortical circuits. Annu Rev Neurosci 2010;33:23–
701 48.

702 24. Monko T, Rebertus J, Stolley J, Salton SR, Nakagawa Y. Thalamocortical axons regulate
703 neurogenesis and laminar fates in the early sensory cortex. Proc Natl Acad Sci U S A
704 2022;119:e2201355119.

705 25. Silver J, Edwards MA, Levitt P. Immunocytochemical demonstration of early appearing astroglial
706 structures that form boundaries and pathways along axon tracts in the fetal brain. J Comp Neurol
707 1993;328:415–36.

708 26. Marcus RC, Blazeski R, Godement P, Mason CA. Retinal axon divergence in the optic chiasm:
709 uncrossed axons diverge from crossed axons within a midline glial specialization. J Neurosci
710 1995;15:3716–29.

711 27. Shu T, Richards LJ. Cortical axon guidance by the glial wedge during the development of the
712 corpus callosum. J Neurosci 2001;21:2749–58.

713 28. Shu T, Li Y, Keller A, Richards LJ. The glial sling is a migratory population of developing neurons.
714 Development 2003;130:2929–37.

715 29. Pires-Neto MA, Braga-De-Souza S, Lent R. Molecular tunnels and boundaries for growing axons in
716 the anterior commissure of hamster embryos. J Comp Neurol 1998;399:176–88.

717 30. Lent R, Uziel D, Baudrimont M, Fallet C. Cellular and molecular tunnels surrounding the forebrain
718 commissures of human fetuses. J Comp Neurol 2005;483:375–82.

719 31. Jouandet ML, Hartenstein V. Basal telencephalic origins of the anterior commissure of the rat. Exp
720 Brain Res 1983;50:183–92.

721 32. Fenlon LR, Suarez R, Lynton Z, Richards LJ. The evolution, formation and connectivity of the
722 anterior commissure. Semin Cell Dev Biol 2021;118:50–9.

723 33. Martin-Lopez E, Meller SJ, Greer CA. Development of piriform cortex interhemispheric
724 connections via the anterior commissure: progressive and regressive strategies. Brain Struct Funct
725 2018;223:4067–85.

726 34. Defilippi P, Di Stefano P, Cabodi S. p130Cas: a versatile scaffold in signaling networks. Trends Cell
727 Biol 2006;16:257–63.

728 35. Deneka A, Korobeynikov V, Golemis EA. Embryonal Fyn-associated substrate (EFS) and CASS4: The
729 lesser-known CAS protein family members. Gene 2015;570:25–35.

730 36. Bouton AH, Riggins RB, Bruce-Staskal PJ. Functions of the adapter protein Cas: signal convergence
731 and the determination of cellular responses. Oncogene 2001;20:6448–58.

732 37. Ruest PJ, Shin NY, Polte TR, Zhang X, Hanks SK. Mechanisms of CAS substrate domain tyrosine
733 phosphorylation by FAK and Src. Mol Cell Biol 2001;21:7641–52.

734 38. Fonseca PM, Shin NY, Brábek J, Ryzhova L, Wu J, Hanks SK. Regulation and localization of CAS
735 substrate domain tyrosine phosphorylation. Cell Signal 2004;16:621–9.

736 39. Donato DM, Ryzhova LM, Meenderink LM, Kaverina I, Hanks SK. Dynamics and mechanism of
737 p130Cas localization to focal adhesions. J Biol Chem 2010;285:20769–79.

738 40. Bargon SD, Gunning PW, O'Neill GM. The Cas family docking protein, HEF1, promotes the
739 formation of neurite-like membrane extensions. Biochim Biophys Acta 2005;1746:143–54.

740 41. Huang Z, Yazdani U, Thompson-Peer KL, Kolodkin AL, Terman JR. Crk-associated substrate (Cas)
741 signaling protein functions with integrins to specify axon guidance during development.
742 Development 2007;134:2337–47.

743 42. Riccomagno MM, Sun LO, Brady CM, Alexandropoulos K, Seo S, Kurokawa M, et al. Cas adaptor
744 proteins organize the retinal ganglion cell layer downstream of integrin signaling. Neuron
745 2014;81:779–86.

746 43. Wong W, Estep JA, Treptow AM, Rajabli N, Jahncke JN, Ubina T, et al. An adhesion signaling axis
747 involving Dystroglycan, β1-Integrin, and Cas adaptor proteins regulates the establishment of the
748 cortical glial scaffold. PLoS Biol 2023;21:e3002212.

749 44. Wang JF, Park IW, Groopman JE. Stromal cell-derived factor-1alpha stimulates tyrosine
750 phosphorylation of multiple focal adhesion proteins and induces migration of hematopoietic
751 progenitor cells: roles of phosphoinositide-3 kinase and protein kinase C. Blood 2000;95:2505–13.

752 45. Evans IM, Yamaji M, Britton G, Pellet-Many C, Lockie C, Zachary IC, et al. Neuropilin-1 signaling
753 through p130Cas tyrosine phosphorylation is essential for growth factor-dependent migration of
754 glioma and endothelial cells. Mol Cell Biol 2011;31:1174–85.

755 46. Liu G, Li W, Gao X, Li X, Jürgensen C, Park HT, et al. p130CAS is required for netrin signaling and
756 commissural axon guidance. J Neurosci 2007;27:957–68.

757 47. Honda H, Nakamoto T, Sakai R, Hirai H. p130(Cas), an assembling molecule of actin filaments,
758 promotes cell movement, cell migration, and cell spreading in fibroblasts. Biochem Biophys Res
759 Commun 1999;262:25–30.

760 48. Gustavsson A, Yuan M, Fällman M. Temporal dissection of beta1-integrin signaling indicates a role
761 for p130Cas-Crk in filopodia formation. J Biol Chem 2004;279:22893–901.

762 49. Aquino JB, Marmigère F, Lallemend F, Lundgren TK, Villar MJ, Wegner M, et al. Differential
763 expression and dynamic changes of murine NEDD9 in progenitor cells of diverse tissues. Gene
764 Expr Patterns 2008;8:217–26.

765 50. Ishino M, Ohba T, Inazawa J, Sasaki H, Ariyama Y, Sasaki T. Identification of an Efs isoform that
766 lacks the SH3 domain and chromosomal mapping of human Efs. Oncogene 1997;15:1741–5.

767 51. Singh MK, Dadke D, Nicolas E, Serebriiskii IG, Apostolou S, Canutescu A, et al. A Novel Cas Family
768 Member, HEPL, Regulates FAK and Cell Spreading. Mol Biol Cell 2008;19:1627–36.

769 52. Vahedi-Hunter TA, Estep JA, Rosette KA, Rutlin ML, Wright KM, Riccomagno MM. Cas Adaptor
770 Proteins Coordinate Sensory Axon Fasciculation. Sci Rep 2018;8:5996.

771 53. Fischer G, Künemund V, Schachner M. Neurite outgrowth patterns in cerebellar microexplant
772 cultures are affected by antibodies to the cell surface glycoprotein L1. J Neurosci 1986;6:605–12.

773 54. Moos M, Tacke R, Scherer H, Teplow D, Früh K, Schachner M. Neural adhesion molecule L1 as a
774 member of the immunoglobulin superfamily with binding domains similar to fibronectin. Nature
775 1988;334:701–3.

776 55. Munakata H, Nakamura Y, Matsumoto-Miyai K, Itoh K, Yamasaki H, Shiosaka S. Distribution and
777 densitometry mapping of L1-CAM immunoreactivity in the adult mouse brain--light microscopic
778 observation. BMC Neurosci 2003;4:7.

779 56. Lendahl U, Zimmerman LB, McKay RD. CNS stem cells express a new class of intermediate
780 filament protein. Cell 1990;60:585–95.

781 57. Lu X, Duan M, Song L, Zhang W, Hu X, Zhao S, et al. Morphological changes of radial glial cells
782 during mouse embryonic development. Brain Res 2015;1599:57–66.

783 58. Gong S, Zheng C, Doughty ML, Losos K, Didkovsky N, Schambra UB, et al. A gene expression atlas
784 of the central nervous system based on bacterial artificial chromosomes. Nature 2003;425:917–
785 25.

786 59. Honda H, Oda H, Nakamoto T, Honda Z, Sakai R, Suzuki T, et al. Cardiovascular anomaly, impaired
787 actin bundling and resistance to Src-induced transformation in mice lacking p130Cas. Nat Genet
788 1998;19:361–5.

789 60. Tronche F, Kellendonk C, Kretz O, Gass P, Anlag K, Orban PC, et al. Disruption of the glucocorticoid
790 receptor gene in the nervous system results in reduced anxiety. Nat Genet 1999;23:99–103.

791 61. López-Bendito G, Molnár Z. Thalamocortical development: how are we going to get there? Nat
792 Rev Neurosci 2003;4:276–89.

793 62. Hanashima C, Molnár Z, Fishell G. Building bridges to the cortex. Cell 2006;125:24–7.

794 63. Gorski JA, Talley T, Qiu M, Puelles L, Rubenstein JLR, Jones KR. Cortical excitatory neurons and glia,
795 but not GABAergic neurons, are produced in the Emx1-expressing lineage. J Neurosci
796 2002;22:6309–14.

797 64. Goebbels S, Bormuth I, Bode U, Hermanson O, Schwab MH, Nave KA. Genetic targeting of
798 principal neurons in neocortex and hippocampus of NEX-Cre mice. Genesis 2006;44:611–21.

799 65. Madisen L, Zwingman TA, Sunkin SM, Oh SW, Zariwala HA, Gu H, et al. A robust and high-
800 throughput Cre reporting and characterization system for the whole mouse brain. Nat Neurosci
801 2010;13:133–40.

802 66. Milner R, Campbell IL. The integrin family of cell adhesion molecules has multiple functions within
803 the CNS. J Neurosci Res 2002;69:286–91.

804 67. Myers JP, Santiago-Medina M, Gomez TM. Regulation of axonal outgrowth and pathfinding by
805 integrin-ECM interactions. Dev Neurobiol 2011;71:901–23.

806 68. Lilja J, Ivaska J. Integrin activity in neuronal connectivity. J Cell Sci 2018;131:jcs212803.

807 69. Jaudon F, Thalhammer A, Cingolani LA. Integrin adhesion in brain assembly: From molecular
808 structure to neuropsychiatric disorders. Eur J Neurosci 2021;53:3831–50.

809 70. Yan L, Cui Z. Integrin β1 and the Repair after Nervous System Injury. Eur Neurol 2023;86:2–12.

810 71. Bixby JL, Harris WA. Molecular mechanisms of axon growth and guidance. Annu Rev Cell Biol
811 1991;7:117–59.

812 72. Renaudin A, Lehmann M, Girault J, McKerracher L. Organization of point contacts in neuronal
813 growth cones. J Neurosci Res 1999;55:458–71.

814 73. Kerstein PC, Nichol RH, Gomez TM. Mechanochemical regulation of growth cone motility. Front
815 Cell Neurosci 2015;9:244.

816 74. Graus-Porta D, Blaess S, Senften M, Littlewood-Evans A, Damsky C, Huang Z, et al. Beta1-class
817 integrins regulate the development of laminae and folia in the cerebral and cerebellar cortex.
818 Neuron 2001;31:367–79.

819 75. Schmid RS, Anton ES. Role of integrins in the development of the cerebral cortex. Cereb Cortex
820 2003;13:219–24.

821 76. Hevner RF, Shi L, Justice N, Hsueh Y, Sheng M, Smiga S, et al. Tbr1 regulates differentiation of the
822 preplate and layer 6. Neuron 2001;29:353–66.

823 77. Spead O, Poulain FE. Trans-Axonal Signaling in Neural Circuit Wiring. Int J Mol Sci 2020;21:5170.

824 78. Vuori K, Hirai H, Aizawa S, Ruoslahti E. Introduction of p130cas signaling complex formation upon
825 integrin-mediated cell adhesion: a role for Src family kinases. Mol Cell Biol 1996;16:2606–13.

826 79. Schwartz MA. Integrin signaling revisited. Trends Cell Biol 2001;11:466–70.

827 80. Takada Y, Ye X, Simon S. The integrins. Genome Biol 2007;8:215.

828 81. Hynes RO. Integrins: versatility, modulation, and signaling in cell adhesion. Cell 1992;69:11–25.

829 82. McCarty JH, Lacy-Hulbert A, Charest A, Bronson RT, Crowley D, Housman D, et al. Selective
830 ablation of alphav integrins in the central nervous system leads to cerebral hemorrhage, seizures,
831 axonal degeneration and premature death. Development 2005;132:165–76.

832 83. Denda S, Reichardt LF. Studies on integrins in the nervous system. Methods Enzymol
833 2007;426:203–21.

834 84. Bourgin C, Murai KK, Richter M, Pasquale EB. The EphA4 receptor regulates dendritic spine
835 remodeling by affecting beta1-integrin signaling pathways. J Cell Biol 2007;178:1295–307.

836 85. Fazeli A, Dickinson SL, Hermiston ML, Tighe RV, Steen RG, Small CG, et al. Phenotype of mice
837 lacking functional Deleted in colorectal cancer (Dcc) gene. Nature 1997;386:796–804.

838 86. Henkemeyer M, Orioli D, Henderson JT, Saxton TM, Roder J, Pawson T, et al. Nuk controls
839 pathfinding of commissural axons in the mammalian central nervous system. Cell 1996;86:35–46.

840 87. Robichaux MA, Chenaux G, Ho HYH, Soskis MJ, Greenberg ME, Henkemeyer M, et al. EphB1 and
841 EphB2 intracellular domains regulate the formation of the corpus callosum and anterior
842 commissure. Dev Neurobiol 2016;76:405–20.

843 88. Kwon YT, Tsai LH, Crandall JE. Callosal axon guidance defects in p35(-/-) mice. J Comp Neurol
844 1999;415:218–29.

845 89. Islam SM, Shinmyo Y, Okafuji T, Su Y, Naser IB, Ahmed G, et al. Draxin, a repulsive guidance protein
846 for spinal cord and forebrain commissures. Science 2009;323:388–93.

847 90. Ito A, Shinmyo Y, Abe T, Oshima N, Tanaka H, Ohta K. Tsukushi is required for anterior commissure
848 formation in mouse brain. Biochem Biophys Res Commun 2010;402:813–8.

849 91. Klingler E, Martin PM, Garcia M, Moreau-Fauvarque C, Falk J, Chareyre F, et al. The cytoskeleton-
850 associated protein SCHIP1 is involved in axon guidance, and is required for piriform cortex and
851 anterior commissure development. Development 2015;142:2026–36.

852 92. Serafini T, Colamarino SA, Leonardo ED, Wang H, Beddington R, Skarnes WC, et al. Netrin-1 is
853 required for commissural axon guidance in the developing vertebrate nervous system. Cell
854 1996;87:1001–14.

855 93. Falk J, Bechara A, Fiore R, Nawabi H, Zhou H, Hoyo-Becerra C, et al. Dual functional activity of
856 semaphorin 3B is required for positioning the anterior commissure. Neuron 2005;48:63–75.

857 94. Sahay A, Molliver ME, Ginty DD, Kolodkin AL. Semaphorin 3F is critical for development of limbic
858 system circuitry and is required in neurons for selective CNS axon guidance events. J Neurosci
859 2003;23:6671–80.

860 95. Dottori M, Hartley L, Galea M, Paxinos G, Polizzotto M, Kilpatrick T, et al. EphA4 (Sek1) receptor
861 tyrosine kinase is required for the development of the corticospinal tract. Proc Natl Acad Sci U S A
862 1998;95:13248–53.

863 96. Suto F, Ito K, Uemura M, Shimizu M, Shinkawa Y, Sanbo M, et al. Plexin-a4 mediates axon-
864 repulsive activities of both secreted and transmembrane semaphorins and plays roles in nerve
865 fiber guidance. J Neurosci 2005;25:3628–37.

866 97. Chen H, Bagri A, Zupicich JA, Zou Y, Stoeckli E, Pleasure SJ, et al. Neuropilin-2 regulates the
867 development of selective cranial and sensory nerves and hippocampal mossy fiber projections.
868 Neuron 2000;25:43–56.

869 98. Giger RJ, Cloutier JF, Sahay A, Prinjha RK, Levengood DV, Moore SE, et al. Neuropilin-2 is required
870 in vivo for selective axon guidance responses to secreted semaphorins. Neuron 2000;25:29–41.

871 99. Abudureyimu S, Asai N, Enomoto A, Weng L, Kobayashi H, Wang X, et al. Essential Role of
872 Linx/Islr2 in the Development of the Forebrain Anterior Commissure. Sci Rep 2018;8:7292.

873 100. Deuel TAS, Liu JS, Corbo JC, Yoo SY, Rorke-Adams LB, Walsh CA. Genetic interactions between
874 doublecortin and doublecortin-like kinase in neuronal migration and axon outgrowth. Neuron
875 2006;49:41–53.

876 101. Tole S, Gutin G, Bhatnagar L, Remedios R, Hébert JM. Development of midline cell types and
877 commissural axon tracts requires Fgfr1 in the cerebrum. Dev Biol 2006;289:141–51.

878 102. Qu Y, Huang Y, Feng J, Alvarez-Bolado G, Grove EA, Yang Y, et al. Genetic evidence that Celsr3 and
879 Celsr2, together with Fzd3, regulate forebrain wiring in a Vangl-independent manner. Proc Natl
880 Acad Sci U S A 2014;111:E2996-3004.

881 103. Tissir F, Bar I, Jossin Y, De Backer O, Goffinet AM. Protocadherin Celsr3 is crucial in axonal tract
882 development. Nat Neurosci 2005;8:451–7.

883 104. López-Bendito G, Flames N, Ma L, Fouquet C, Di Meglio T, Chedotal A, et al. Robo1 and Robo2
884 cooperate to control the guidance of major axonal tracts in the mammalian forebrain. J Neurosci
885 2007;27:3395–407.

886 105. Hua ZL, Jeon S, Caterina MJ, Nathans J. Frizzled3 is required for the development of multiple axon
887 tracts in the mouse central nervous system. Proc Natl Acad Sci U S A 2014;111:E3005-3014.

888 106. Shen Y, Mani S, Donovan SL, Schwob JE, Meiri KF. Growth-associated protein-43 is required for
889 commissural axon guidance in the developing vertebrate nervous system. J Neurosci
890 2002;22:239–47.

891 107. Chen L, Liao G, Waclaw RR, Burns KA, Linquist D, Campbell K, et al. Rac1 controls the formation of
892 midline commissures and the competency of tangential migration in ventral telencephalic
893 neurons. J Neurosci 2007;27:3884–93.

894 108. Stein E, Huynh-Do U, Lane AA, Cerretti DP, Daniel TO. Nck recruitment to Eph receptor,
895 EphB1/ELK, couples ligand activation to c-Jun kinase. J Biol Chem 1998;273:1303–8.

896 109. Stein E, Lane AA, Cerretti DP, Schoecklmann HO, Schroff AD, Van Etten RL, et al. Eph receptors
897 discriminate specific ligand oligomers to determine alternative signaling complexes, attachment,
898 and assembly responses. Genes Dev 1998;12:667–78.

899 110. Huynh-Do U, Stein E, Lane AA, Liu H, Cerretti DP, Daniel TO. Surface densities of ephrin-B1
900 determine EphB1-coupled activation of cell attachment through alphavbeta3 and alpha5beta1
901 integrins. EMBO J 1999;18:2165–73.

902 111. Becker E, Huynh-Do U, Holland S, Pawson T, Daniel TO, Skolnik EY. Nck-interacting Ste20 kinase
903 couples Eph receptors to c-Jun N-terminal kinase and integrin activation. Mol Cell Biol
904 2000;20:1537–45.

905 112. Suh LH, Oster SF, Soehrman SS, Grenningloh G, Sretavan DW. L1/Laminin modulation of growth
906 cone response to EphB triggers growth pauses and regulates the microtubule destabilizing protein
907 SCG10. J Neurosci 2004;24:1976–86.

908 113. Xu NJ, Henkemeyer M. Ephrin-B3 reverse signaling through Grb4 and cytoskeletal regulators
909 mediates axon pruning. Nat Neurosci 2009;12:268–76.

910 114. Tolner EA, Sheikh A, Yukin AY, Kaila K, Kanold PO. Subplate neurons promote spindle bursts and
911 thalamocortical patterning in the neonatal rat somatosensory cortex. J Neurosci 2012;32:692–
912 702.

913 115. Viswanathan S, Bandyopadhyay S, Kao JPY, Kanold PO. Changing microcircuits in the subplate of
914 the developing cortex. J Neurosci 2012;32:1589–601.

915 116. Molnár Z, Adams R, Goffinet AM, Blakemore C. The role of the first postmitotic cortical cells in the
916 development of thalamocortical innervation in the reeler mouse. J Neurosci 1998;18:5746–65.

917 117. Gilmore EC, Ohshima T, Goffinet AM, Kulkarni AB, Herrup K. Cyclin-dependent kinase 5-deficient
918 mice demonstrate novel developmental arrest in cerebral cortex. J Neurosci 1998;18:6370–7.

919 118. Belvindrah R, Graus-Porta D, Goebbels S, Nave KA, Müller U. Beta1 integrins in radial glia but not
920 in migrating neurons are essential for the formation of cell layers in the cerebral cortex. J Neurosci
921 2007;27:13854–65.

922 119. O'Leary DD, Schlaggar BL, Tuttle R. Specification of neocortical areas and thalamocortical
923 connections. Annu Rev Neurosci 1994;17:419–39.

924 120. Molnár Z, Adams R, Blakemore C. Mechanisms underlying the early establishment of
925 thalamocortical connections in the rat. J Neurosci 1998;18:5723–45.

926 121. Kanold PO, Kara P, Reid RC, Shatz CJ. Role of subplate neurons in functional maturation of visual
927 cortical columns. Science 2003;301:521–5.

928 122. Kanold PO. Subplate neurons: crucial regulators of cortical development and plasticity. Front
929 Neuroanat 2009;3:16.

930 123. Hoerder-Suabedissen A, Molnár Z. Morphology of mouse subplate cells with identified projection
931 targets changes with age. J Comp Neurol 2012;520:174–85.

932 124. Ohtaka-Maruyama C. Subplate Neurons as an Organizer of Mammalian Neocortical Development.
933 Front Neuroanat 2020;14:8.

934 125. Cabodi S, del Pilar Camacho-Leal M, Di Stefano P, Defilippi P. Integrin signalling adaptors: not only
935 figurants in the cancer story. Nat Rev Cancer 2010;10:858–70.

936 126. Machiyama H, Hirata H, Loh XK, Kanchi MM, Fujita H, Tan SH, et al. Displacement of p130Cas from
937 focal adhesions links actomyosin contraction to cell migration. J Cell Sci 2014;127:3440–50.

938 127. Seo S, Asai T, Saito T, Suzuki T, Morishita Y, Nakamoto T, et al. Crk-associated substrate lymphocyte
939 type is required for lymphocyte trafficking and marginal zone B cell maintenance. J Immunol
940 2005;175:3492–501.

941 128. Donlin LT, Danzl NM, Wanjalla C, Alexandropoulos K. Deficiency in expression of the signaling
942 protein Sin/Efs leads to T-lymphocyte activation and mucosal inflammation. Mol Cell Biol
943 2005;25:11035–46.

944 129. Wu SX, Goebbels S, Nakamura K, Nakamura K, Kometani K, Minato N, et al. Pyramidal neurons of
945 upper cortical layers generated by NEX-positive progenitor cells in the subventricular zone. Proc
946 Natl Acad Sci U S A 2005;102:17172–7.

947 130. Wang F, Flanagan J, Su N, Wang LC, Bui S, Nielson A, et al. RNAscope: a novel in situ RNA analysis
948 platform for formalin-fixed, paraffin-embedded tissues. J Mol Diagn 2012;14:22–9.

949

950

951 **Figure Legends**

952 **Figure 1. p130Cas protein is expressed in the developing cortex during lamination and white**
953 **matter tract formation.** (**A-I'**) Immunohistochemistry showing the developmental expression
954 pattern of p130Cas protein (green) during cortical development of WT mice. At E14.5, p130Cas
955 expression is strongly detected in the intermediate zone and marginal zone and more diffusely
956 in the cortical plate (**C-C'**). At E16.5, p130Cas expression is strongest in the cortical white matter,
957 intermediate zone, subventricular zone, and marginal zone (**F-F'**). By E18.5, p130Cas is broadly
958 expressed throughout the cortex, with stronger expression in the subventricular, marginal, and
959 intermediate zones (**I-I'**). Robust co-expression of p130Cas with axonal marker NCAM-L1 (red) is
960 observed in cortical white matter tracts, including the External Capsule (EC) (**B, E, and H**, white
961 arrowhead) and the Anterior Commissure (AC) (**B, F, and H**, white arrows). MZ = Marginal Zone;
962 CP = Cortical Plate; IZ = Intermediate Zone; SVZ = Subventricular Zone; VZ = Ventricular Zone.
963 Scale bar = 250µm (A-B', D-I'). Scale bar = 100µm (C-D'). E14.5: n = 4; E16.5: n = 3; and E18.5: n =
964 4.

965

966 **Figure 2. *p130Cas* is expressed in neurons that project axons along the cortical white matter.**
967 (**A-E''**) Detection of EGFP (green) expression of *p130Cas-EGFP-BAC* transgenic mice co-
968 immunolabeled with the axonal marker NCAM-L1 (red) at E14.5 (**A-A''**), E16.5 (**B-B''**), and P0 (**C-**
969 **C''**). Analysis reveals strong *p130Cas* promoter activity during the formation of cortical white
970 matter tracts. Robust EGFP expression is observed in the External Capsule (EC) (**A, B, C**, white
971 arrowhead) and Anterior Commissure (AC) (**A, B, C**, white arrows). High-resolution images at P0

972 show EGFP (**D', E'**) and NCAM-L1 (**D'', E''**) expression at the pallial-subpallial boundary (PSPB) (**D**,
973 dotted line) and the cortical plate (**E**). Scale bar = 250µm. n = 3 animals for each developmental
974 timepoint.

975

976 **Figure 3. *Cas TcKO* mutants display errors in cortical and thalamocortical connections. (A-B'')**
977 Immunohistological analysis of major cortical tracts using the axonal marker NCAM-L1 (green) in
978 *Nes-Cre;TcKO* mutant and control neonates (P0). Two major defasciculation phenotypes are
979 present in *Nes-Cre;TcKO* mice: 1) efferents originating in the cortex fail to fasciculate properly in
980 the pAC tract and erroneously project into the subpallium (**B'**), and 2) thalamocortical
981 connections meant to innervate layer IV mis-project to the subpial boundary, forming large
982 Cortical Bundles (**B''**). Each of these phenotypes is fully penetrant in *Nes-Cre;TcKO* mutants. The
983 high-magnification panel in **B''** is from a similar area as the upper box in **B**, but from a nearby
984 section. (**C-H**) The origin of mis-projecting axons is confirmed via anterograde lipophilic tracing
985 experiments. DiA crystals placed into the S2 cortex label ventrally defasciculating AC axons (**D**,
986 arrowheads) but not Cortical Bundles (**F**) in *Nes-Cre;TcKO* mutants. DiI crystals placed in the
987 laterodorsal thalamus label Cortical Bundles (**H**, white asterisks). (**I**) Quantification of the
988 number of stray axon bundles in the subpallial area. Unpaired *t*-test, ***$p < 0.001$, n = 7 for *Nes-*
989 *Cre;TcKO,* n = 10 for controls. (**J**) Quantification of the number of Cortical Bundles. Unpaired *t-*
990 test, ****$p < 0.0001$, n = 8 for *Nes-Cre;TcKO,* n = 7 for controls. Values provided are mean ±
991 SEM. Scale bar = 250µm.

992

993 **Figure 4. Developmental progression of white matter defects in *Nes-Cre;TcKO* mutants.** (**A-F''**)
994 Immunohistochemistry for the axonal marker NCAM-L1 (green) in *Nes-Cre;TcKO* mutants and
995 control mice at E14.5 (**A-B''**), E16.5 (**C-D''**), and E18.5 (**E-F''**). Analysis reveals different
996 developmental timelines for each defasciculation phenotype. The EC-AC tract begins developing
997 at E14.5 in control (**A'**) and *Nes-Cre;TcKO* mice (**B'**). *Nes-Cre;TcKO* mice display no AC
998 defasciculation errors until E18.5 (**F'**, white arrowhead). Cortical Bundles are apparent at E14.5
999 in *Nes-Cre;TcKO* mutants (**B''**, white asterisks) and worsen in severity as development continues
1000 (**D''** and **F''**, white asterisks). (**G**) Quantification of the average number of stray axon bundles in
1001 the subpallial area at E18.5. Unpaired *t*-test, **$p < 0.01$, n = 5 for *Nes-Cre;TcKO,* n = 4 for
1002 controls. (**H**) Quantification of the average number of Cortical Bundles at E14.6, E16.5, and
1003 E18.5. Two-way ANOVA, $p < 0.0001$; Tukey HSD post hoc test, ****$p < 0.0001$ E14.5 *Nes-*
1004 *Cre;TcKO* versus control, E16.5 *Nes-Cre;TcKO* versus control, E18.5 *Nes-Cre;TcKO* versus control,
1005 E14.5 *Nes-Cre;TcKO* versus E18.5 *Nes-Cre;TcKO*, E16.5 *Nes-Cre;TcKO* versus E18.5 *Nes-Cre;TcKO*;
1006 ns E14.5 *Nes-Cre;TcKO* vs E16.5 *Nes-Cre;TcKO*; E14.5: n = 4 for *Nes-Cre;TcKO,* n = 4 for controls;
1007 E16.5: n = 8 for *Nes-Cre;TcKO,* n = 12 for controls; E18.5: n = 5 for *Nes-Cre;TcKO,* n = 4 for
1008 controls). Values provided are mean ± SEM. Scale bar = 250µm.

1009

1010 **Figure 5. Neuronal-autonomous and non-neuronal autonomous roles for *Cas* genes in white**
1011 **matter tract fasciculation.** (**A-H''**) Immunohistochemistry for the axonal marker NCAM-L1
1012 (green) in *Emx1-Cre;TcKO* and *Nex-Cre;TcKO* neonates. Analysis reveals both classes of
1013 conditional knockouts present the AC defasciculation phenotype (**B' and H'**, white arrowheads),
1014 indicating this phenotype is neuronal-autonomous (i.e, Cas proteins function within the neurons

1015 themselves). This phenotype is fully penetrant in *Emx1-Cre;TcKO* and *Nex-Cre;TcKO* mutants.
1016 Similar to *Nes-Cre;TcKO* mutants (**Figure 2**), defasciculating axons in the subpallial area of *Emx1-*
1017 *Cre;TcKO* and *Nex-Cre;TcKO* mutants are cortical in origin as revealed by anterograde DiA tracing
1018 from crystal placement in the S2 cortex (**D and J**, white arrowheads). In contrast, only *Emx1-*
1019 *Cre;TcKO* mutants display the Cortical Bundle phenotype (**B''**, white asterisks). Cortical Bundles
1020 are confirmed to be TCA projections by anterograde labeling from DiI crystals placed in the
1021 laterodorsal thalamus (**F**, white asterisks). The absence of the Cortical Bundle phenotype in *Nex-*
1022 *Cre;TcKO* mutants (**H'' and L**) indicates *Cas* genes function in a population of cortical non-
1023 neuronal cells during TCA fasciculation and projection. (**M**) Quantification of the number of
1024 stray axon bundles in the subpallial area in *Emx1-Cre;TcKO* mutants and controls. Unpaired *t-*
1025 test, ****$p < 0.0001$, n = 8 for *Emx1-Cre;TcKO,* n = 10 for controls. (**N**) Quantification of the
1026 number of Cortical Bundles in *Emx1-Cre;TcKO* mutants and controls. Unpaired *t*-test, ****$p <$
1027 0.0001, n = 8 for *Emx1-Cre;TcKO,* n = 10 for controls. (**O**) Quantification of the number of stray
1028 axon bundles in the subpallial area of *Nex-Cre;TcKO* mutants and controls. Unpaired *t*-test,
1029 ****$p < 0.0001$, n = 8 for *Nex-Cre;TcKO,* n = 7 for controls. Values provided are mean ± SEM.
1030 Scale bar = 250µm.

1031

1032 **Figure 6. Genetic labeling confirms cortical origins of AC defasciculating axons in *Cas TcKO***
1033 **mutants.** (**A-H''**) Immunohistochemistry for NCAM-L1 (green) and the tdTomato fluorescent
1034 Cre-dependent reporter (red). Analysis reveals extensive co-labeling in defasciculating AC axon
1035 bundles in both *Emx1-Cre;Ai14$^{+/-}$;TcKO* (**C-D''**) and *Nex-Cre;Ai14$^{+/-}$;TcKO* (**G-H''**) mutants. In both
1036 classes of conditional mutants, tdTomato+ defasciculating axons appear to intercalate with

1037 diffuse NCAM-L1+ processes that occupy the subpallium (**D' vs D'' and H' vs H''**, white
1038 arrowheads). No tdTomato+ processes may be seen invading the subpallium in *Emx1-Cre;Ai14*$^{+/-}$
1039 *;CasL*$^{+/-}$*;Sin*$^{+/-}$*;p130Cas*$^{+/+}$ controls (**A-B''**) and *Nex-Cre;Ai14*$^{+/-}$*;CasL*$^{+/-}$*;Sin*$^{+/-}$*;p130Cas*$^{+/+}$ (**E-F''**)
1040 controls. (**I**) Quantification of the number of stray axon bundles in the subpallial area of *Emx1-*
1041 *Cre;Ai14*$^{+/-}$*;TcKO* mutants and controls. Unpaired *t*-test, ****p < 0.0001, n = 3 for *Emx1-*
1042 *Cre;Ai14*$^{+/-}$*;TcKO*, n = 3 for controls. (**J**) Quantification of the number of stray axon bundles in the
1043 subpallial area of *Nex-Cre;Ai14*$^{+/-}$*;TcKO* mutants and controls. Unpaired *t*-test, *p < 0.05, n = 4 for
1044 *Nex-Cre;Ai14*$^{+/-}$*;TcKO,* n = 3 for controls. Values provided are mean ± SEM. Scale bar = 250µm.

1045

1046 **Figure 7. *Itgb1* mutants phenocopy the TCA tract defects observed in *Cas TcKO* mutants. (A-**
1047 **D'')** Immunohistological analysis of NCAM-L1 (green) in *Emx1-Cre;Itgb1*$^{fl/fl}$ and *Nex-Cre;Itgb1*$^{fl/fl}$
1048 neonates. Neither class of conditional mutant phenocopies the AC defasciculation defects
1049 observed in *Cas TcKO* mutants (**B' and D'**), suggesting that β1-integrin is dispensable for AC tract
1050 fasciculation. Only *Emx1-Cre;Itgb1*$^{fl/fl}$ mutants phenocopy the Cortical Bundle phenotype
1051 observed in *Cas TcKO* mutants (**B''**, white asterisks), indicating β1-integrin similarly functions in
1052 a population of cortical non-neuronal cells during TCA projection. (**E**) Quantification of the
1053 number of Cortical Bundles in *Emx1-Cre;Itgb1*$^{fl/fl}$ mutants and controls. Unpaired *t*-test, ****p <
1054 0.0001, n = 6 for *Emx1-Cre;Itgb1*$^{fl/fl}$*,* n = 5 for controls. Values provided are mean ± SEM. Scale
1055 bar = 250µm.

1056

1057 **Figure 8. Cortical Bundle phenotype in E16.5 *Itgb1* and *Cas TcKO* mutants correlates with**
1058 **displaced subplate cells. (A-H'')** Immunohistochemistry of Tbr1 (red) and NCAM-L1 (green) in
1059 E16.5 *Emx1-Cre;TcKO* and *Emx1-Cre;Itgb1*$^{fl/fl}$ mutants. Analysis reveals that severe cortical
1060 dysplasia is associated with Cortical Bundles. In both classes of conditional mutants, Tbr1+
1061 deep-layer/subplate cells are displaced to more superficial layers (**D' and H'**, white asterisks).
1062 Cortical Bundles correlate with superficially displaced Tbr1+ deep-layer/subplate cells (**D''** and
1063 **H''**, white asterisks). 100% penetrance and expressivity. n = 6 for *Emx1-Cre;TcKO*, n = 6 for
1064 controls; n = 8 for *Emx1-Cre;Itgb1,* n = 8 for controls. Scale bar = 250µm.

1065

1066 **Figure 9. Cortical Bundle phenotype in P0 *Itgb1* and *Cas TcKO* neonate mutants correlates with**
1067 **displaced subplate cells. (A-H'')** Immunohistological analysis of Tbr1 (red) and NCAM-L1 (green)
1068 in P0 *Emx1-Cre;TcKO* and *Emx1-Cre;Itgb1*$^{fl/fl}$ mutants. Severe cortical dysplasia is associated with
1069 Cortical Bundles. In both classes of conditional mutants, Tbr1+ deep-layer/subplate cells are
1070 displaced to more superficial positions (**D' and H'**, white asterisks). Cortical Bundles correlate
1071 with superficially displaced Tbr1+ deep-layer/subplate cells (**D'' and H''**, white asterisks). 100%
1072 penetrance and expressivity. n = 5 for *Emx1-Cre;TcKO*, n = 7 for controls; n = 6 for *Emx1-*
1073 *Cre;Itgb1*, n = 5 for controls. Scale bar = 250µm.

1074

1075 **S1 Table. Numerical values for graphs in Figure 3, Figure 4, Figure 5, Figure 6, and Figure 7.** The
1076 number of stray axon bundles in the subpallial area and the number of CBs in the cortex for

1077 each section from each animal analyzed. Data are organized by figure: **Fig 3** (Sheet 1), **Fig 4**
1078 (Sheet 2), **Fig 5** (Sheet 3), **Fig 6** (Sheet 4), and **Fig 7** (Sheet 5).

1079

1080 **S1 Fig. p130Cas protein is expressed in the developing neocortex.** (**A-F'**)
1081 Immunohistochemistry showing the developmental expression pattern of p130Cas protein
1082 (green) during wild-type cortical development. At E14.5, p130Cas protein expression overlapped
1083 with the radial glial cell marker Nestin (red) in the cortical plate and at the pial surface (**B-B'**). At
1084 E16.5, p130Cas expression is strongest in the cortical white matter, subventricular zone, and
1085 marginal zone (**D-D'**). By E18.5, p130Cas is robustly expressed in the subventricular and
1086 intermediate zones (**F-F'**). Weaker expression of p130Cas is also detected at the marginal zone
1087 and pial surface at E16.5 (**D'**) and E18.5 (**F'**), overlapping with Nestin expression (**D and F**). MZ =
1088 Marginal Zone; CP = Cortical Plate; IZ = Intermediate Zone; SVZ = Subventricular Zone; VZ =
1089 Ventricular Zone. Scale bar = 250µm (A, C-F'). Scale bar = 100µm (B-B'). E14.5: n = 4; E16.5: n =
1090 3; and E18.5: n = 4.

1091

1092 **S2 Fig. The p130Cas antibody is specific for p130Cas protein.** (**A-H'**) Immunohistochemistry of
1093 E16.5 *Nes-Cre;TcKO* and littermate control embryos (*CasL*$^{-/-}$*;Sin*$^{-/-}$*;p130Cas*$^{fl/+}$) demonstrates
1094 p130Cas signal (green) is not detected in *Nes-Cre;TcKO* mice. Control embryos strongly
1095 express p130Cas protein in the developing neocortex (**D'**) and cortical white matter tracts (**A'**),
1096 including the External Capsule (EC) and Anterior Commissure (AC) (**B'**). p130Cas signal is lost in
1097 *Nes-Cre;TcKO* embryos (**E'**, **F'**, and **H'**) except for in the hypothalamic region (**E'** and **G'**, white

1098 asterisk). Note that the expression of p130Cas looks nearly identical in control *CasL*$^{-/-}$*;Sin*$^{-/-}$

1099 *;p130Cas*$^{fl/+}$ embryos and wild-type embryos (**Fig 1**; **S1 Fig**). MZ = Marginal Zone; CP = Cortical

1100 Plate; IZ = Intermediate Zone; SVZ = Subventricular Zone; VZ = Ventricular Zone. Scale bar =

1101 250µm (A-A', C-C', E-E', and G-G'). Scale bar = 100µm (B-B', D-D', F-F', and H-H'). n = 3 animals for

1102 *Nes-Cre;TcKO* and control.

1103

1104 **S3 Fig. Placement of DiA and DiI crystals in *Nes-Cre;TcKO* mutants and controls.** (**A-F**) DiA and

1105 DiI crystal placement in coronal sections from P0 *Nes-Cre;TcKO* and control mice. DiA crystals

1106 were placed into the Somatosensory 2 (S2) region of the cortex (**C**), while DiI crystals were

1107 placed along the central region of the thalamus (**F**). Scale bar = 250µm.

1108

1109 **S4 Fig. Illustration of cell-type-specific requirements of *Cas* gene function for TCA pathfinding.**

1110 **(A-C)** Representative model depicting the differences in *Cas* gene expression in Control, *Emx1-*

1111 *Cre;TcKO*, and *Nex-Cre;TcKO* animals. (**A**) In control animals, *Cas* genes are expressed in radial

1112 glial cells (RGCs; solid blue), postmitotic immature migrating neurons (solid yellow), and post-

1113 migratory excitatory cortical neurons (solid grey), including the subplate (solid red). (**B**) *Emx1-*

1114 *Cre* drives recombination in cortical RGCs. Thus, in *Emx1-Cre;TcKO* mutants, *Cas* genes are

1115 ablated in RGCs (hollow blue), immature migrating excitatory neurons (hollow yellow), and

1116 excitatory neurons (hollow grey), including the subplate (hollow red). Thalamocortical axons

1117 (TCAs) project to mispositioned subplate cells, resulting in the Cortical Bundle (CB) phenotype

1118 observed in *Emx1-Cre;TcKO* mutant mice. (**C**) In *Nex-Cre;TcKO* animals, *Nex-Cre* drives

1119 recombination in early postmitotic excitatory cortical neurons. *Cas* genes are therefore present
1120 in RGCs (solid blue), but not in migrating neurons (hollow yellow) and post-migratory neurons of
1121 the developing neocortex (hollow grey and hollow red). TCA projections are normal in *Nex-*
1122 *Cre;TcKO* mutants. ECM = Extracellular Matrix; MZ = Marginal Zone; CP = Cortical Plate; VZ =
1123 Ventricular Zone; RGC = Radial Glial Cell; TCA = Thalamocortical Axons. Created with
1124 BioRender.com.

1125

1126 **S5 Fig. Rabbit anti-β1-integrin antibody is not specific for β1-integrin protein.** (**A-F'**)
1127 Immunohistochemistry of E16.5 *Emx1-Cre;Itgb1* and littermate control animals using the rabbit-
1128 anti-β1-integrin antibody (Cell Signaling Technology) demonstrates that putative β1-integrin
1129 signal (green) is still present in the cortex of *Emx1-Cre;Itgb1* mice. Control embryos show signal
1130 in the marginal zone (**C'**), cortical plate, and all major cortical white matter tracts (**A'**), including
1131 thalamocortical axons (**C'**), the External Capsule (EC) (**E'**), and the Anterior Commissure (AC) (**E'**).
1132 This signal is still observed in *Emx1-Cre;Itgb1* animals, including the cortical plate, EC, and AC
1133 (**B'**, **D', and F'**). Scale bar = 250µm (A-A' and B-B'). Scale bar = 100µm (C-F'). n = 4 animals for
1134 *Emx1-Cre;Itgb1* and control.

1135

1136 **S6 Fig. Mouse anti-β1-integrin antibody is not specific for β1-integrin protein.** (**A-F'**)
1137 Immunohistochemistry of E16.5 *Emx1-Cre;Itgb1* and littermate control animals using the
1138 mouse-anti-β1-integrin antibody (eBioscience) shows that putative β1-integrin signal (green) is
1139 still present in the cortex of *Emx1-Cre;Itgb1* mice. Control embryos show signal in the

1140 vasculature (**C'**), the piriform cortex (**E'**), marginal zone, and all major cortical white matter
1141 tracts (**A'**), including thalamocortical axons (**C'**) and the External Capsule (EC) (**E'**) and Anterior
1142 Commissure (AC) (**E'**). Strong signal is still detected in the cortex, AC, and EC of *Emx1-Cre;Itgb1*
1143 animals (**B'**). High-magnification images show clear β1-integrin signal in thalamocortical axons
1144 (**D'**) and the EC and AC (**F'**). Scale bar = 250µm (**A-A' and B-B'**). Scale bar = 100µm (C-F'). n = 4
1145 animals for *Emx1-Cre;Itgb1* and control.

1146

1147 **S7 Fig. *Itgb5*, *Itgb6*, and *Itgb8* are expressed in the neocortex at E14.5.** (**A-D'''**) RNAScope for
1148 *Itgb5* (yellow), *Itgb6* (magenta), and *Itgb8* (cyan) in the developing neocortex at E14.5. *Itgb6* is
1149 expressed diffusely throughout the developing neocortex (**A'', B'', and C''**), while *Itgb8* is
1150 robustly expressed in the subventricular and ventricular zones of the Primary Somatosensory
1151 Cortex (S1) (**B'''**) and Secondary Somatosensory Cortex (S2) (**C'''**). *Itgb5* appears to be weakly
1152 expressed in the ventricular zone as well as in the vasculature (**A'**). High magnification images
1153 show diffuse expression of *Itgb6* (**D''**) and *Itgb8* (**D'''**) in the Piriform Cortex (P). S1 = Primary
1154 Somatosensory Cortex; S2 = Secondary Somatosensory Cortex; P = Piriform Cortex. MZ =
1155 Marginal Zone; CP = Cortical Plate; IZ = Intermediate Zone; SVZ = Subventricular Zone; VZ =
1156 Ventricular Zone. Scale bar = 250µm (A-A'''). Scale bar = 100µm (B-D'''). n = 3 animals.

1157

1158 **S8 Fig. *Itgb5*, *Itgb6*, and *Itgb8* are expressed in the neocortex at E16.5.** (**A-D'''**) RNAScope for
1159 *Itgb5* (yellow), *Itgb6* (magenta), and *Itgb8* (cyan) in the developing neocortex at E16.5. *Itgb5*,
1160 *Itgb6*, and *Itgb8* are all expressed in the ventricular zone of the Primary Somatosensory Cortex

1161 (S1) (**B'-B'''**) and Secondary Somatosensory Cortex (S2) (**C'-C'''**). *Itgb5* also appears to be
1162 expressed in the vasculature (**A'**). Weak expression of *Itgb6* (**B''**) and *Itgb8* (**B'''**) is detected in
1163 the marginal zone of S1 and S2. Expression of *Itgb6* (**D''**) and *Itgb8* (**D'''**) is observed in the
1164 Piriform Cortex (P). S1 = Primary Somatosensory Cortex; S2 = Secondary Somatosensory Cortex;
1165 P = Piriform Cortex. MZ = Marginal Zone; CP = Cortical Plate; IZ = Intermediate Zone; SVZ =
1166 Subventricular Zone; VZ = Ventricular Zone. Scale bar = 250µm (A-A'''). Scale bar = 100µm (B-
1167 D'''). n = 3 animals.

1168

1169 **S9 Fig. *Itgb5*, *Itgb6*, and *Itgb8* are expressed in the neocortex at E18.5.** (**A-D'''**) RNAScope for
1170 *Itgb5* (yellow), *Itgb6* (magenta), and *Itgb8* (cyan) in the developing neocortex at E18.5. All three
1171 transcripts are strongly expressed in the ventricular zone of the Primary Somatosensory Cortex
1172 (S1) (**B', B'', and B'''**). *Itgb5* appears to be weakly expressed in the vasculature (**B', C', and D'**).
1173 *Itgb8* is diffusely expressed in the Secondary Somatosensory Cortex (S2) (**C'''**). Expression of
1174 *Itgb6* (**D''**) and *Itgb8* (**D'''**) is detected in the Piriform Cortex (P). S1 = Primary Somatosensory
1175 Cortex; S2 = Secondary Somatosensory Cortex; P = Piriform Cortex. MZ = Marginal Zone; CP =
1176 Cortical Plate; IZ = Intermediate Zone; SVZ = Subventricular Zone; VZ = Ventricular Zone. Scale
1177 bar = 250µm (A-A'''). Scale bar = 100µm (B-D'''). n = 3 animals.

1178

1179 **S10 Fig. Positioning of deep-layer neurons is normal in P0 *Nex-Cre;TcKO* animals.** (**A-D''**)
1180 Immunohistochemistry of P0 *Nex-Cre;TcKO* animals using the axonal marker NCAM-L1 (green)
1181 and the deep layer marker Tbr1 (red) shows no apparent differences in lamination between

1182 *NexCre;TcKO* and control cortices. Normal positioning of deep-layer/subplate cells is observed in

1183 *Nex-Cre;TcKO* animals (**D'**). This correlated with the normal fasciculation and pathfinding of

1184 NCAM-L1+ (green) cortical white matter tracts. n = 4 for *Nex-Cre;TcKO* and controls. Scale bar =

1185 250µm (A and C). Scale bar = 100µm (B-B'', D-D'').

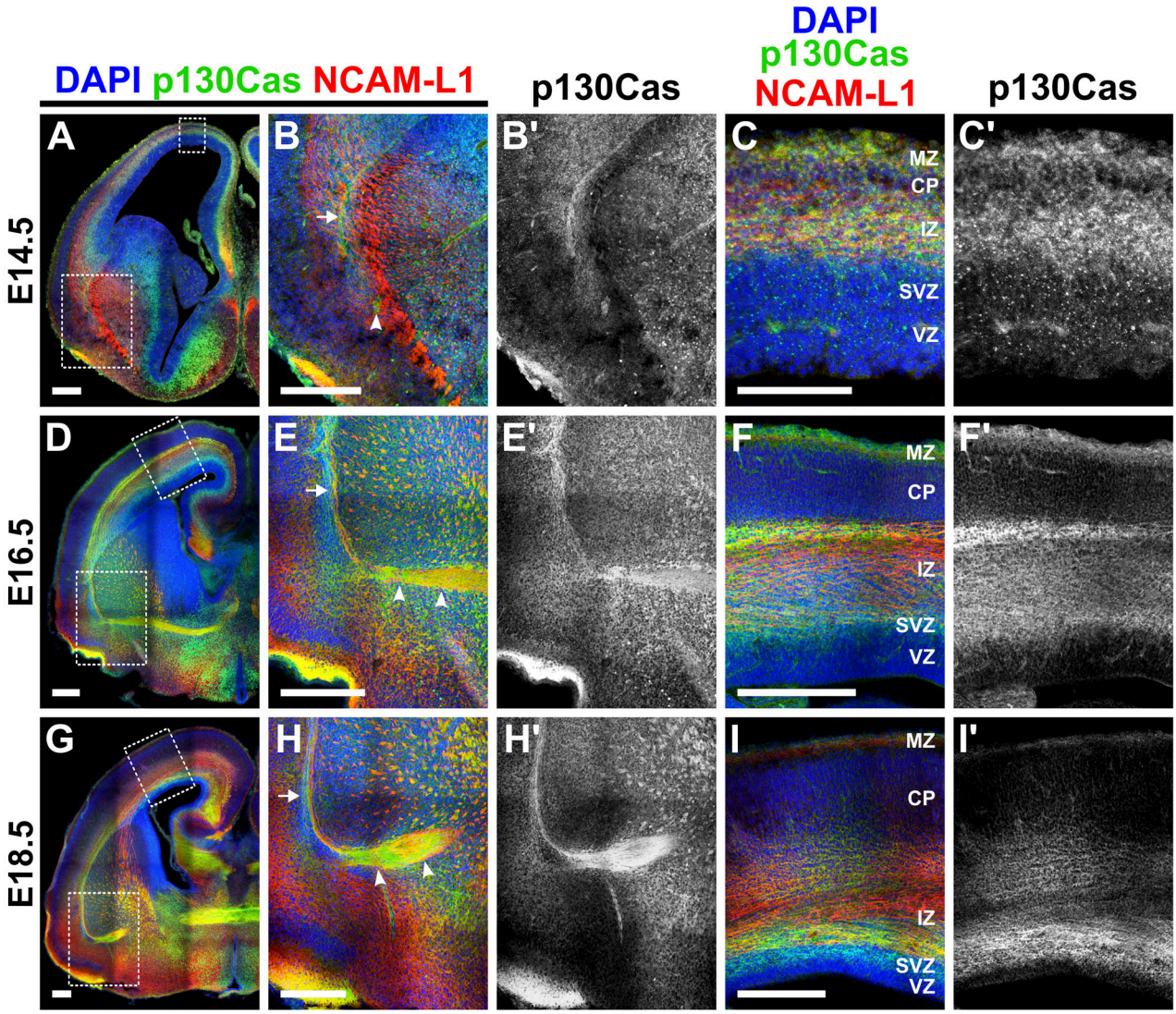
DAPI p130Cas NCAM-L1
p130Cas
DAPI
p130Cas
NCAM-L1
p130Cas
E14.5
E16.5
E18.5
A
B
B'
C
C'
D
E
E'
F
F'
G
H
H'
I
I'
MZ
CP
IZ
SVZ
VZ

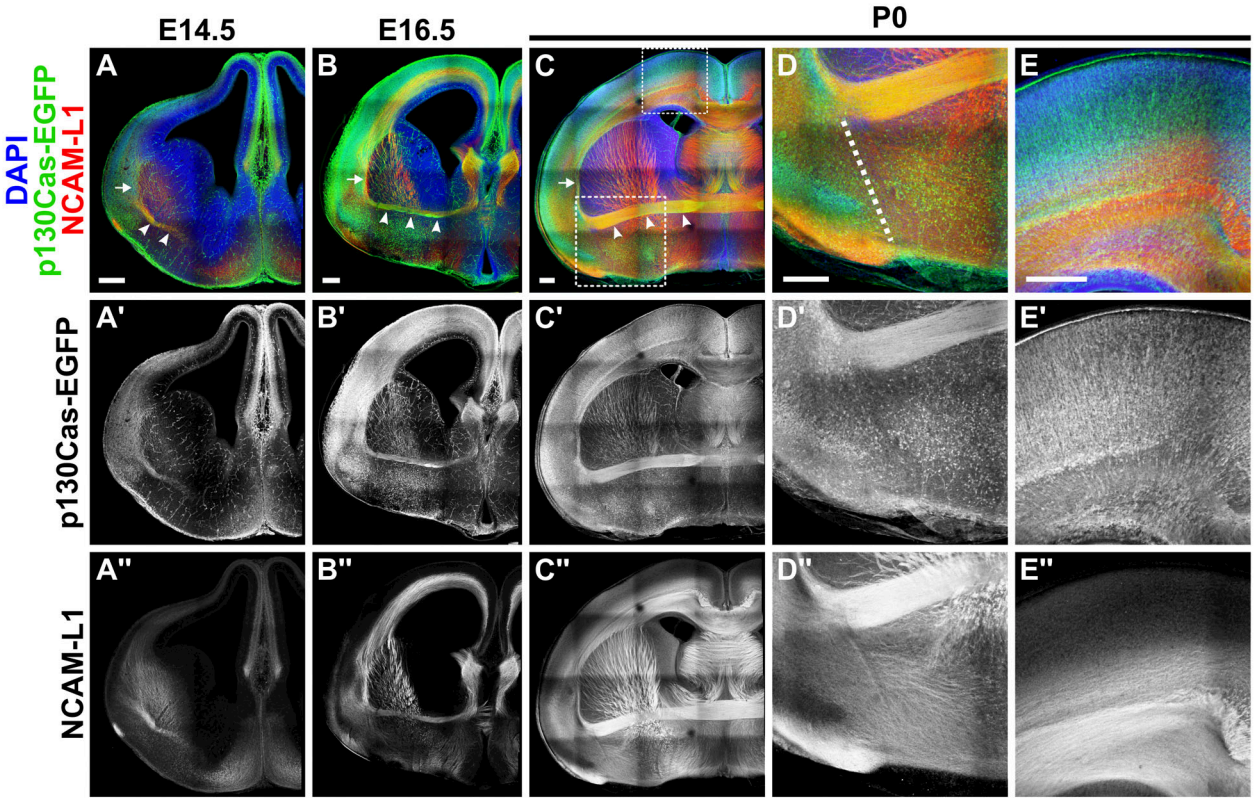
E14.5
E16.5
P0
DAPI
p130Cas-EGFP
NCAM-L1
A
B
C
D
E
A'
B'
C'
D'
E'
A''
B''
C''
D''
E''
p130Cas-EGFP
NCAM-L1

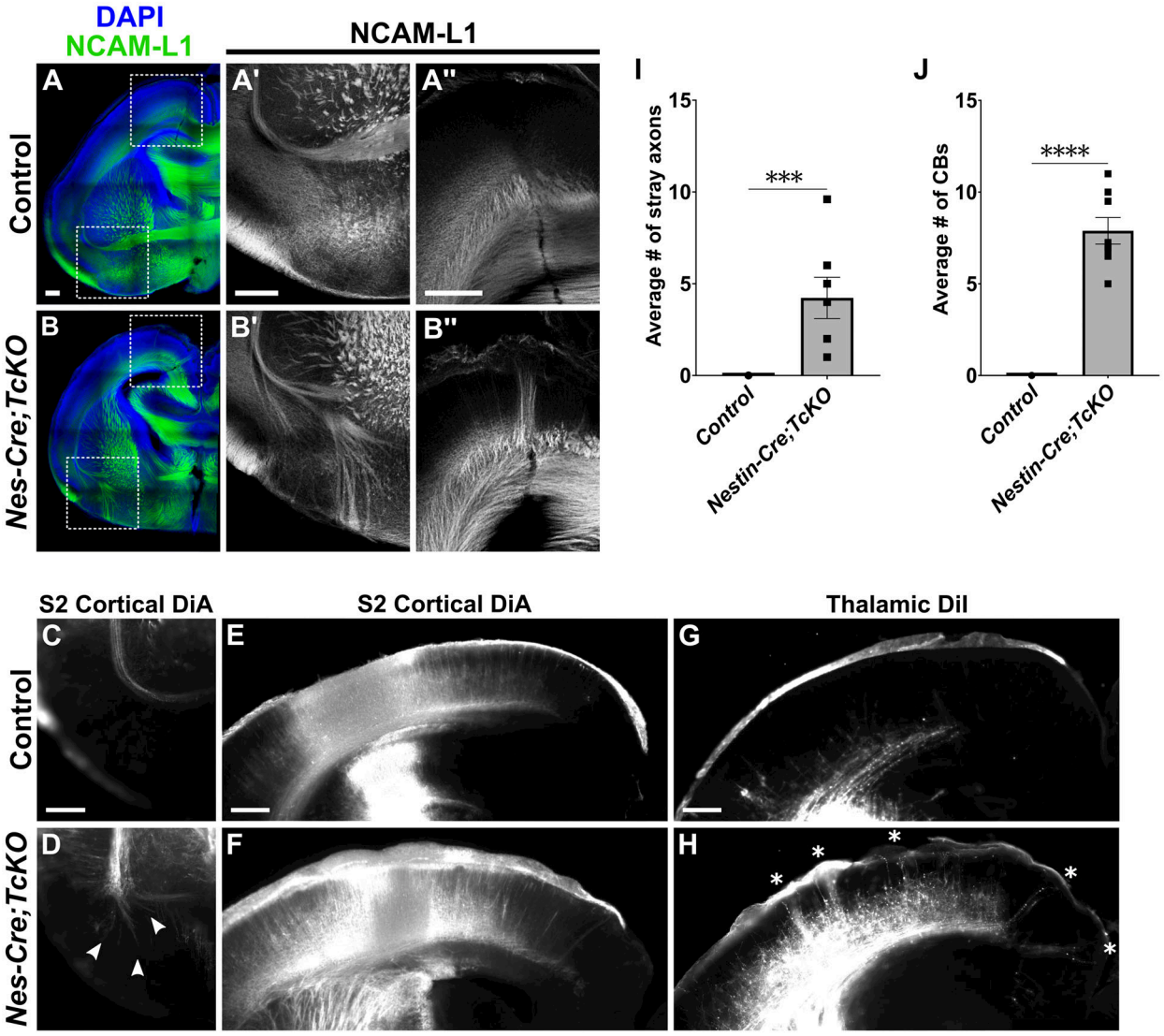
DAPI
NCAM-L1
NCAM-L1
A
A'
A''
B
B'
B''
Control
Nes-Cre;TcKO
I
J
Average # of stray axons
Average # of CBs
***
****
Control
Nestin-Cre;TcKO
S2 Cortical DiA
S2 Cortical DiA
Thalamic DiI
C
E
G
D
F
H
Control
Nes-Cre;TcKO

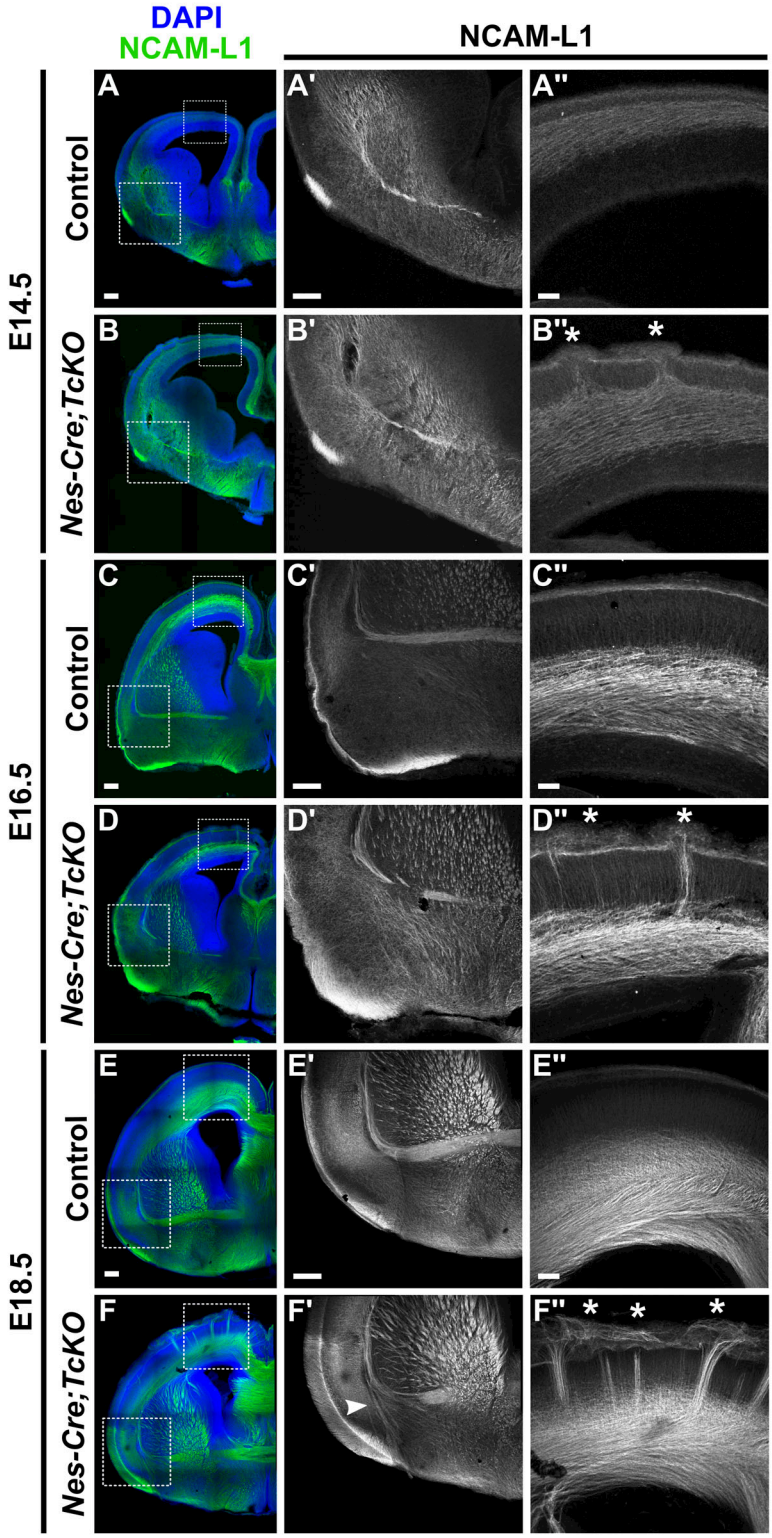
DAPI
NCAM-L1
NCAM-L1
E14.5
E16.5
E18.5
Control
Nes-Cre;TcKO
A
A'
A''
B
B'
B''
C
C'
C''
D
D'
D''
E
E'
E''
F
F'
F''

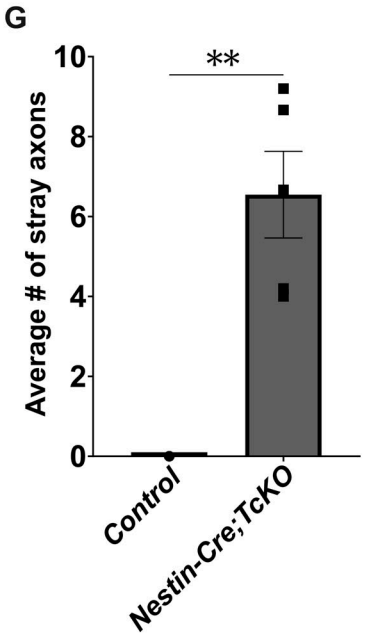
G
Average # of stray axons
10
8
6
4
2
0
**
Control
Nestin-Cre;TcKO

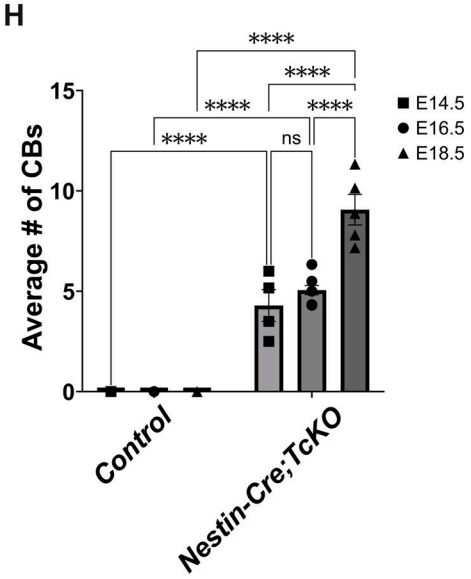
H
Average # of CBs
15
10
5
0
****
****
****
****
****
ns
E14.5
E16.5
E18.5
Control
Nestin-Cre;TcKO

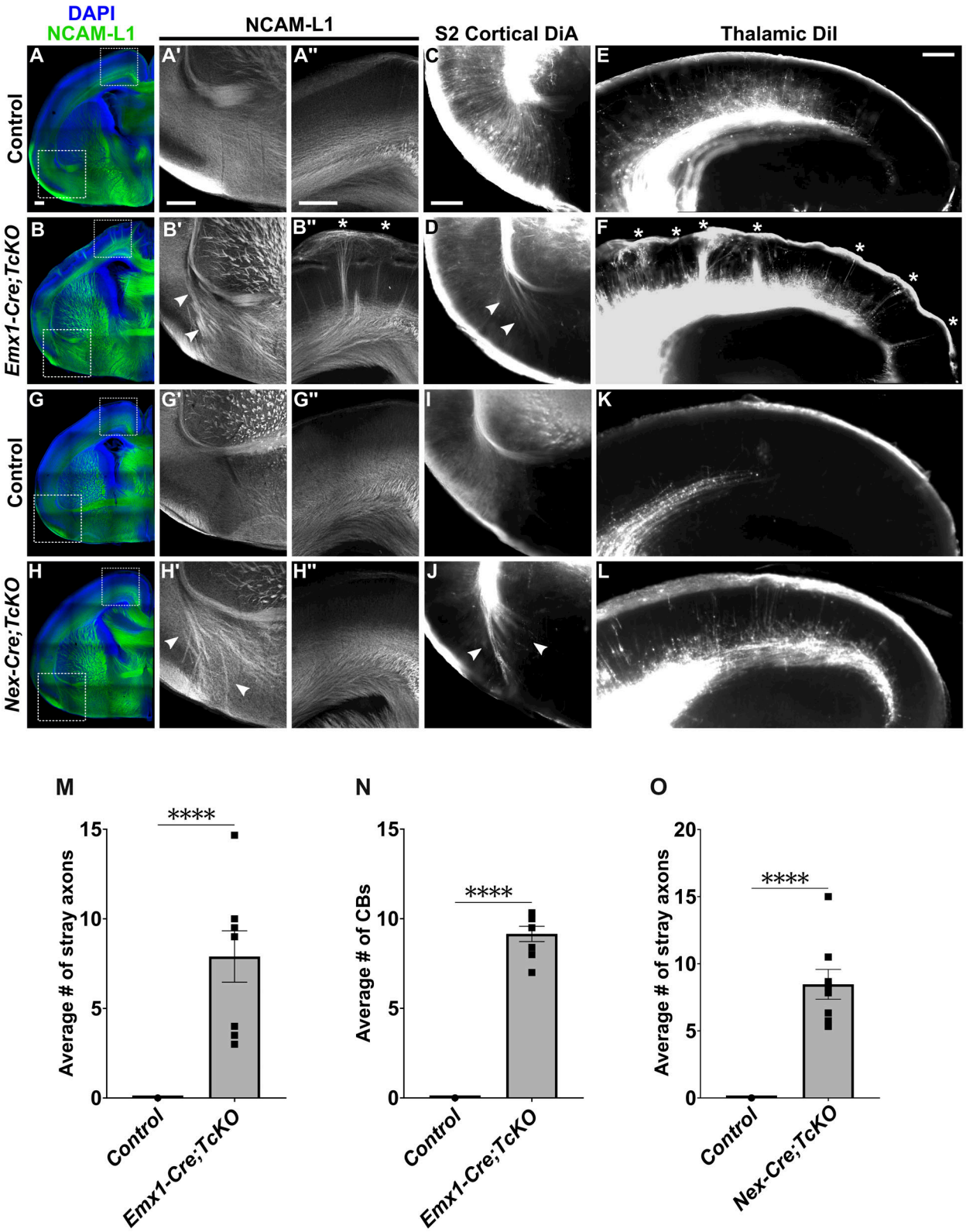
DAPI
NCAM-L1
NCAM-L1
S2 Cortical DiA
Thalamic DiI
Control
Emx1-Cre;TcKO
Control
Nex-Cre;TcKO
A
A'
A''
C
E
B
B'
B''
D
F
G
G'
G''
I
K
H
H'
H''
J
L
M
N
O
Average # of stray axons
Average # of CBs
Average # of stray axons
****
****
****
Control
Emx1-Cre;TcKO
Control
Emx1-Cre;TcKO
Control
Nex-Cre;TcKO

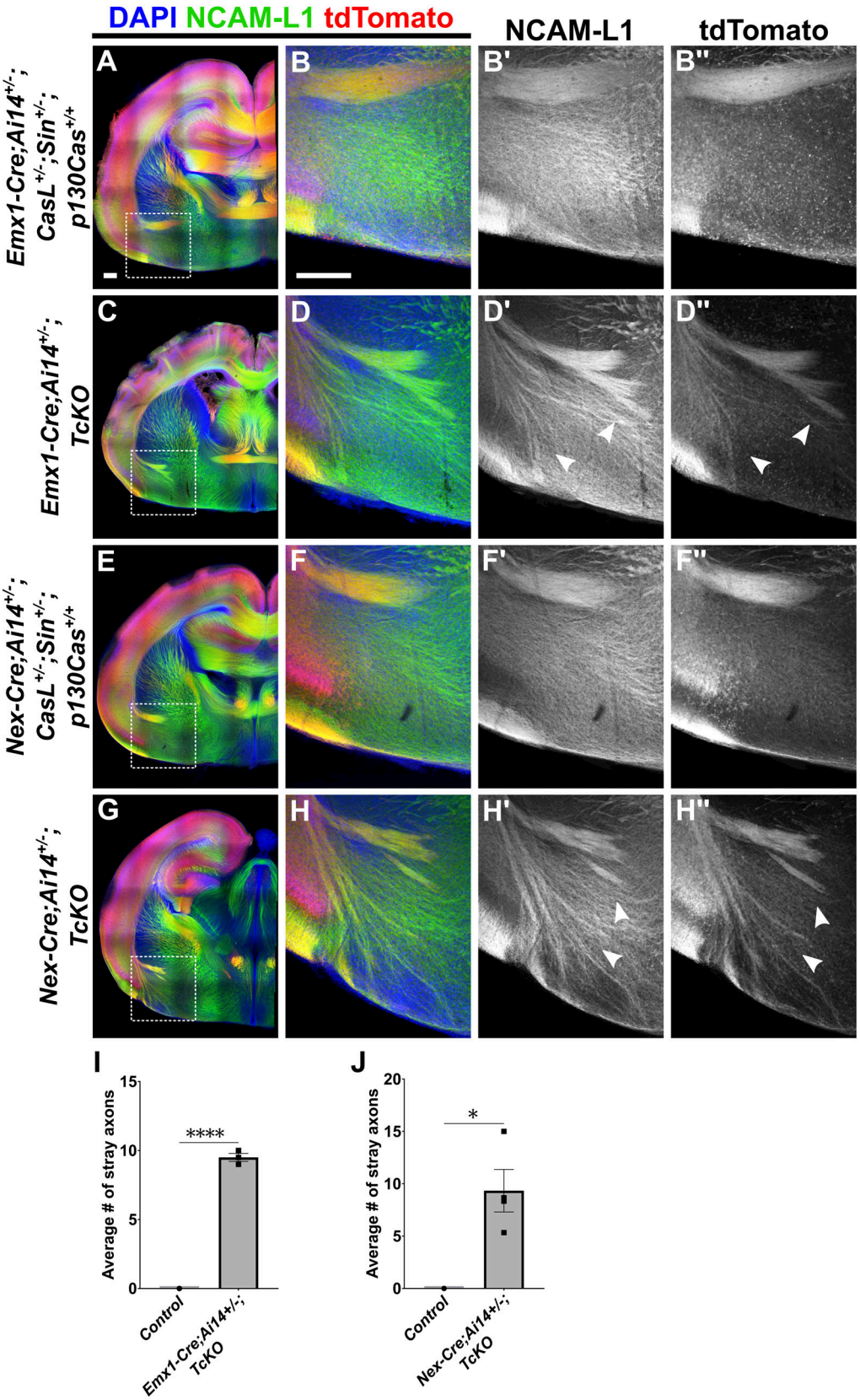
DAPI NCAM-L1 tdTomato
NCAM-L1
tdTomato
Emx1-Cre;Ai14+/-; CasL+/-;Sin+/-; p130Cas+/+
Emx1-Cre;Ai14+/-; TcKO
Nex-Cre;Ai14+/-; CasL+/-;Sin+/-; p130Cas+/+
Nex-Cre;Ai14+/-; TcKO
A
B
B'
B''
C
D
D'
D''
E
F
F'
F''
G
H
H'
H''
I
Average # of stray axons
****
Control
Emx1-Cre;Ai14+/-; TcKO
J
Average # of stray axons
*
Control
Nex-Cre;Ai14+/-; TcKO

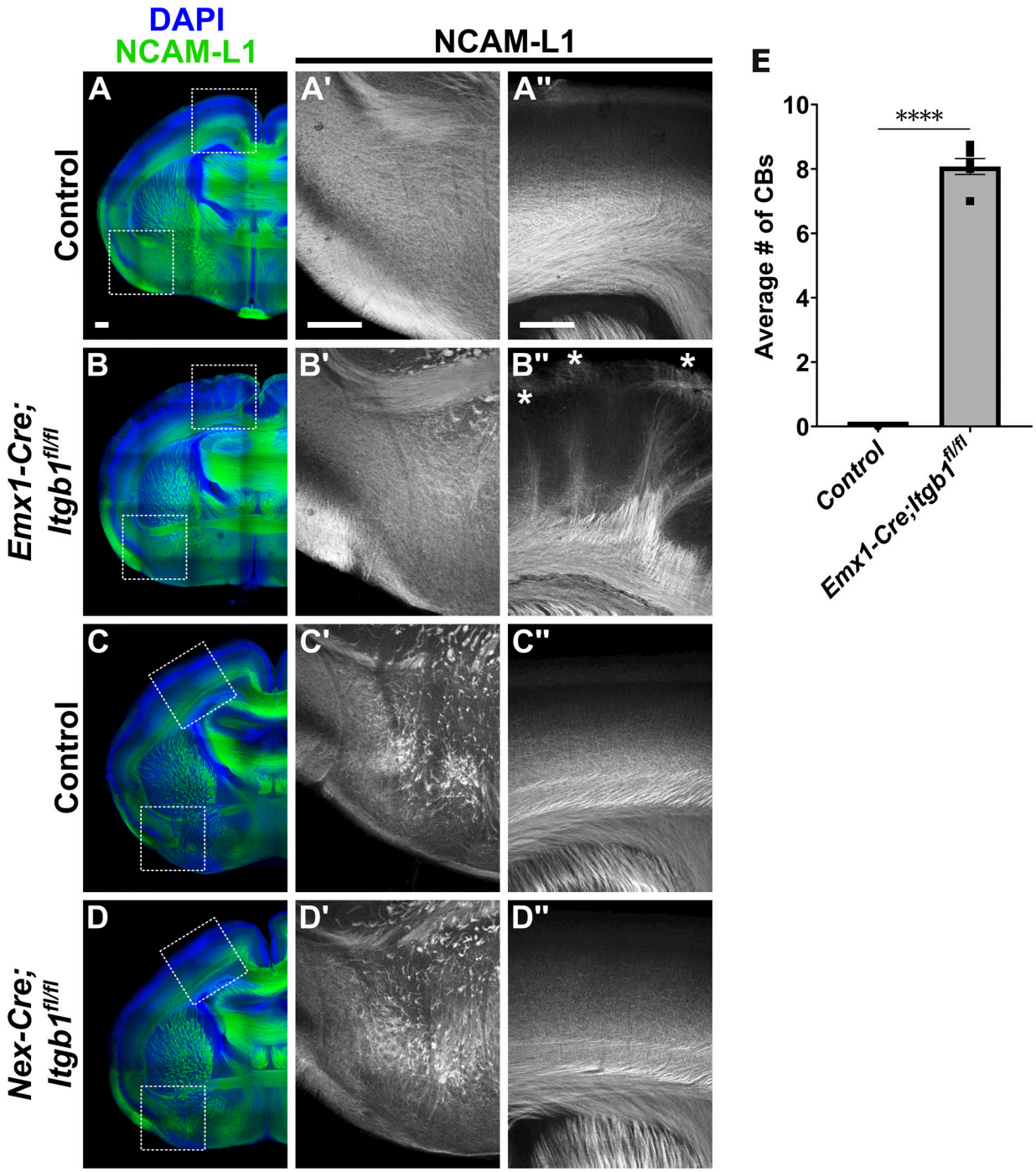
DAPI
NCAM-L1
NCAM-L1
A
A'
A''
Control
B
B'
B''
Emx1-Cre; Itgb1fl/fl
C
C'
C''
Control
D
D'
D''
Nex-Cre; Itgb1fl/fl
E
Average # of CBs
10
8
6
4
2
0
****
Control
Emx1-Cre;Itgb1fl/fl

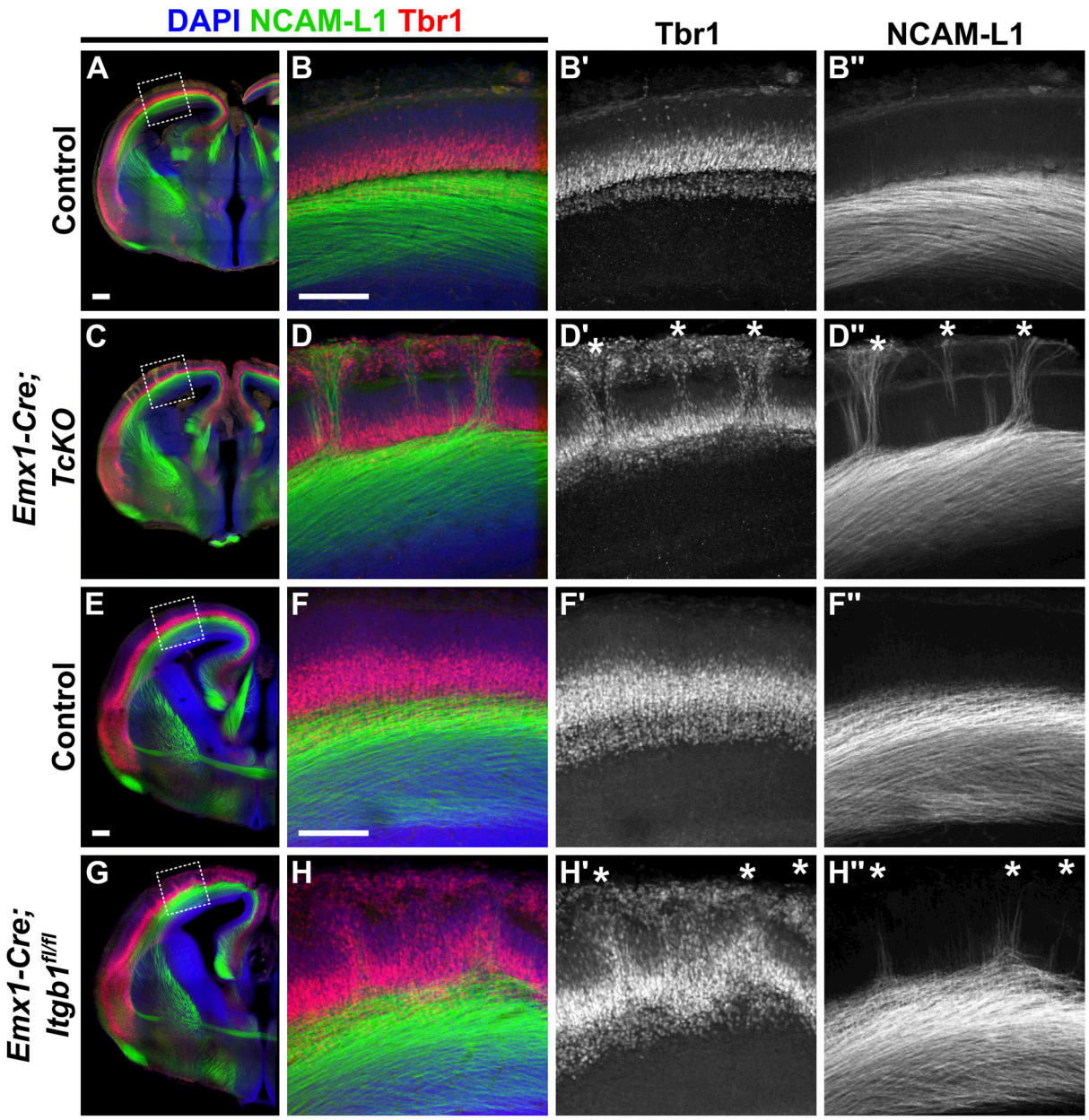
DAPI NCAM-L1 Tbr1
Tbr1
NCAM-L1
Control
Emx1-Cre; TcKO
Control
Emx1-Cre; Itgb1fl/fl
A
B
B'
B''
C
D
D'
D''
E
F
F'
F''
G
H
H'
H''

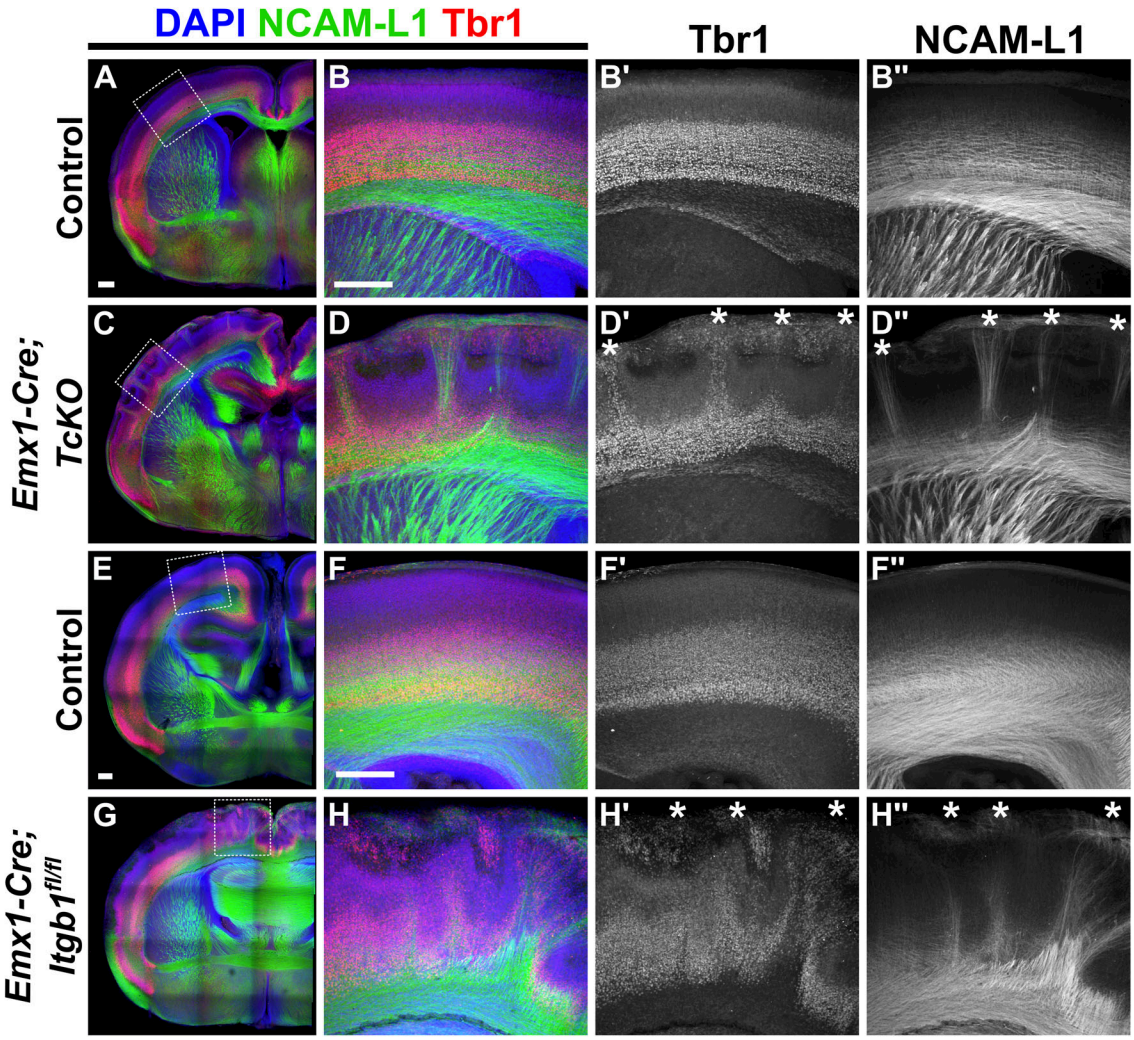
DAPI NCAM-L1 Tbr1
Tbr1
NCAM-L1
Control
Emx1-Cre; TcKO
Control
Emx1-Cre; Itgb1fl/fl
A
B
B'
B''
C
D
D'
D''
E
F
F'
F''
G
H
H'
H''